Journal of Environmental Chemical Engineering 13 (2025) 120416

Contents lists available at ScienceDirect

Journal of Environmental Chemical Engineering

journal homepage: www.elsevier.com/locate/jece

Highly efficient and selective one-step production of glycidol from glycerol using Cs/zeolite catalysts in a packed-bed reactor

Andrii Kostyniuk *, Anže Prašnikar, Blaž Likozar

Department of Catalysis and Chemical Reaction Engineering, National Institute of Chemistry, Hajdrihova 19, Ljubljana 1001, Slovenia

ARTICLE INFO

Keywords:
Catalytic dehydrative epoxidation
Glycerol conversion
Glycidol production
CsNO3—doped H-ZSM-5 zeolite material
Reaction optimization

ABSTRACT

In this work, the one-step gas-phase conversion of glycerol to glycidol was achieved and optimized over $CsNO_3$-modified ZSM-5 zeolite catalysts (SiO_2/Al_2O_3 = 1500) with varying Cs loadings (5–30 wt%) in a packed-bed reactor. To the best of our knowledge, our group's work remains the only study of its kind reported in the literature. Increasing the reaction temperature from 350 to 450 °C enhanced both catalytic activity and glycidol selectivity, whereas further temperature elevation led to a decline in both selectivity and space-time yield (STY). The highest glycidol selectivity of 74.0 C% was achieved over the granulated 15Cs/ZSM-5 catalyst at 350 °C after 8 h of time-on-stream (TOS) using a 10 wt% glycerol feed. A maximum glycidol yield of 61.1 C% and the highest STY of 2.5 $mmol \cdot g_{cat}^{-1} \cdot h^{-1}$ were achieved at glycerol concentrations of 20 and 40 wt%, respectively. The superior performance of the 15Cs/ZSM-5 catalyst is attributed to its favorable morphology (enhanced pore diameter), high basicity, and selective dehydrative-epoxidation activity, likely facilitated by Cs-induced modification of the zeolite surface and local restructuring at the pore entrances. Although glycerol conversion gradually decreased during long-term testing, glycidol selectivity remained relatively stable over 70 h of continuous operation. Overall, this study demonstrates the development of a high-performing, regenerable catalyst with strong industrial application potential and provides mechanistic insights into the design of effective systems for the one-step synthesis of glycidol from glycerol.

1. Introduction

Glycerol (propane-1,2,3-triol) is a valuable biomass-derived compound and represents the major byproduct of biodiesel production, contributing approximately 67 % to the global glycerol supply [1,2]. While biodiesel offers environmental benefits, its economic feasibility is hindered when compared to regular petrodiesel due to challenges in using carbon atoms from the starting materials and the higher cost of vegetable oils compared to fossil fuels. To encourage its use, various governments provide incentives, such as reduced sales taxes. These measures aim to reduce the reliance on fossil fuels and adhere to regulations requiring the partial replacement of traditional fuels with bio-based options in the short to medium term. This trend is observed in different countries, including the European Union and the United States. A comprehensive study by the International Energy Agency [3] reveals a consistent increase in biodiesel production from 2019 to 2025, with Europe leading the global charge in this field (Fig. 1).

Within the process of making biodiesel, glycerol emerges as a significant byproduct, making up around 10 % of the total biodiesel produced. The surplus of glycerol has caused its commercial value to decrease due to its widespread availability in the global market. The production of glycidol from glycerol is attractive pathway. Glycidol, also known as 2,3-epoxy-1-propanol, is a highly reactive compound with epoxide and alcohol behaviour and can be miscible with water but also reacts with it and decomposes when distilled at atmospheric pressure. It is known that glycidol undergoes explosive decomposition in the presence of strong acids or bases, salts or metals and effected spontaneous polymerization under heat or exposure of impurities which results to utilize 70 wt% of isopropanol for its transportation [4]. In 1909, chemist N. Prilezhaev at the University of Warsaw synthesized glycidol via epoxidation of allyl alcohol with peroxybenzoic acid which became the breakthrough reaction at the time and was called the Prilezhaev oxidation [5]. Glycidol is still produced in a similar way through epoxidation of allyl alcohol with hydrogen peroxide over tungsten-derived catalysts (Scheme 1**a**) [6].

Another alternative pathway is production of glycidol from glycerol through the obtaining of 3-chloro-1,2-propanediol using HCl and NaOH and titanium silicate (TS-1) as a catalyst. All these methods are non-

* Corresponding author.
E-mail address: andrii.kostyniuk@ki.si (A. Kostyniuk).

https://doi.org/10.1016/j.jece.2025.120416
Received 12 September 2025; Received in revised form 11 November 2025; Accepted 20 November 2025
Available online 21 November 2025

environmentally friendly and unsustainable, moreover they are including multiple steps, high production cost (expensive purification steps and equipment corrosion), and produced of large amount of waste liquid and salts. Recently, our group [7] obtained glycidol via one-step dehydrative epoxidation reaction from aqueous solution of glycerol in a packed-bed reactor in N_2 atmosphere under ambient pressure (Scheme 1**c**).

According to the latest research by Growth Market Reports, the global glycidol market was valued at approximately USD 210 million in 2024 [8]. It is expected to grow steadily at a compound annual growth rate (CAGR) of 5.7 % between 2025 and 2033, reaching an estimated value of around USD 350 million by 2033. The final price of glycidol is affected by its purity, which is an important factor. The most widely used and requested purity level for glycidol is 96 %, as it is utilized in cosmetic preparations, laundry detergents, disinfectants, and is increasingly being used in products such as skin creams, shampoos, moisturizing lotions, and so on. In addition, glycidol is utilized in the stabilization of natural oils and vinyl polymers, and also serves as a chemical intermediate in the synthesis of glycidyl ethers, esters, and amines [9].

Zeolites, which are aluminosilicate molecular sieves, are highly useful as catalysts and catalyst supports [10]. The discovery of ZSM-5 in 1967 has facilitated the development of significant processes like dewaxing, methanol to gasoline, and olefin oligomerization [11]. For instance, Merck and Co. has pilot plant scale related to a basic-zeolite-catalyzed process for the synthesis of 4-methyl thiazol in the gas phase over cesium sulfate impregnated into ZSM-5 catalyst with high hydrothermal stability in the presence of water vapor at 723–773 K [10].

In addition, the dehydrative epoxidation of ethylene glycol, 1,2-propanediol, and 2,3-butanediol into epoxyethane, 1,2-epoxypropane, and 2,3-epoxybutane over alkali metal oxides (Ca, Mg, Cs, Sr, K and Na) supported on SiO_2 were investigated by Kim and co-authors [12]. Interestingly, the authors established that Cs/SiO_2 is the most promising catalyst with outstanding performance for the dehydrative epoxidation of 2,3-butanediol. This catalyst activity was explained by strong basic sites formed by Cs ion and its strong interaction with SiO_2 support, high accessibility of the reactant to basic sites due to low penetration of Cs ions into SiO_2 and finally the presence of mild acidic surface on SiO_2 which is favourite for water elimination. Also Kim et al. [13] determined that the dehydrative epoxidation of 2,3-butanediol on a Cs/SiO_2 catalyst primarily involves the reactivity of basic sites.

In our previous work [7], we successfully demonstrated the one-step gas-phase conversion of glycerol to glycidol over Cs/ZSM-5 catalysts, achieving a maximum glycidol yield of 40.4 %. In the present study, we further advance this concept by employing $CsNO_3$-modified ZSM-5 catalysts with optimized performance, achieving a significantly higher glycidol yield of 61.1 %. A comprehensive investigation was conducted to understand the influence of various parameters, including Cs loading, reaction temperature, time, pressure, glycerol concentration, and catalyst granulation. Moreover, catalyst deactivation, regeneration, and long-term stability were systematically evaluated, providing valuable insights into catalyst design and reaction mechanisms.

2. Experimental section

2.1. Catalyst synthesis

H-ZSM-5 zeolite with the SiO_2/Al_2O_3 ratio of 1500 was purchased from Tosoh Corp. (HSZ-890HOA). The synthesis of Cs/ZSM-5 catalysts with different loading of Cs was carried out by the impregnation of H-ZSM-5 zeolite using the wet impregnation method with 0.005–0.05 M solution of cesium nitrate ($CsNO_3$). First, H-ZSM-5 zeolite was calcined at 550 °C in air for 6 h to completely remove any organic residues from the protonated form. Thereafter, 100–500 mL of $CsNO_3$ solution was added to the corresponding zeolite with vigorous stirring for 2–3 h at 80 °C. Then the samples were dried overnight at 110 °C and calcined at 550 °C for 6 h in static air with a heating rate 10 °C. Thereafter, these synthesized catalysts were ground. 6 different catalysts supported by parent H-ZSM-5 zeolite were synthesized and studied, namely: 5Cs/ZSM-5, 10/CsZSM-5, 15Cs/ZSM-5, 20Cs/ZSM-5, 25Cs/ZSM-5, and 30Cs/ZSM-5.

2.2. Catalyst characterization

Textural properties of the catalysts were measured by the N_2 adsorption-desorption method on a Micromeritics ASAP 2020 instrument. Before the experiment, the sample (150 mg) was degassed at 200 °C overnight (temperature ramp 10 °C/min) under vacuum (10^{-3} Pa), and afterward, an N_2 adsorption-desorption analysis was carried out at −196 °C, while the pore-size distribution was calculated based on the desorption isotherms by the Barrett-Joyner-Halenda (BJH) method and the total surface area was calculated by the Brunauer-Emmett-Teller (BET) method.

The solid phase catalysts composition was identified by powder X-

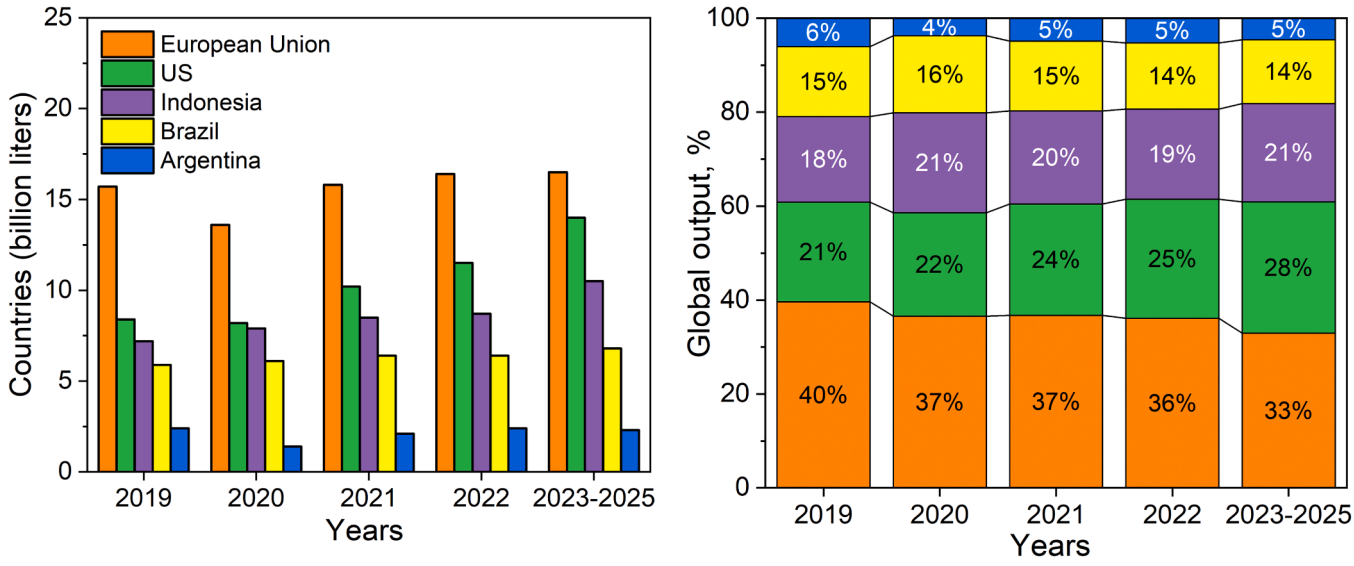

Fig. 1. Global biodiesel and hydrotreated vegetable oil (HVO) production trends by key markets (2019–2025), as documented by the International Energy Agency [3].

ray diffraction analysis on PANalytical XpertPro instrument using CuKα1 radiation (1.54056 Å) in the range of 2 theta angles ranging from 5° to 90° with increments of 0.034°. The average crystallite size was calculated using the Scherrer equation and based on the most significant peaks at 7.9°, 8.8°, 23.1°, 23.3°, 23.9°, 24.5°. The determination of the relative crystallinity values was based on the intensity of the same 6 characteristic MFI peaks [7].

The element content was determined by inductively coupled plasma mass spectroscopy (ICP-MS) using an Agilent 7500ce. Before the analysis, the samples were fumed with a mixture of HF and $HClO_4$. The residue was dissolved in the mixture of HCl and H_3BO_4 and diluted for determination of the Cs content in catalyst samples. The amount of carbon in the studied spent catalysts was quantified using TGA-FTIR (thermogravimetric analysis-infrared spectrometry) Spectrum 3 with EGA 4000 from PerkinElmer. The analysis of the spent catalysts was performed in the temperature range from 40 to 750 °C with a heating rate of 10 °C/min in an air stream with a flow rate of 100 mL/min.

A scanning electron microscope (SEM) (FE–SEM SUPRA 35–F, Carl Zeiss) equipped with an energy-dispersive spectrometer Inca 400 (Oxford Instruments) was used to record the morphology of the studied catalysts, while the particle size of each sample was calculated from the obtained HRSEM images using the ImageJ software. Scanning transmission electron microscopy (STEM) micrographs and energy dispersive X-ray spectroscopy (EDXS) chemical mapping of the samples were obtained using a JEOL ARM 200 CF microscope with a cold field-emission gun and Jeol Centurio EDXS system [14].

The basicity of the catalysts was also determined using of Hammett indicator and benzoic acid titration [15–17]. The indicator selected for titration was bromothymol blue for the base strength H_7.2. Briefly, 0.5 g of catalysts was put into a 100 mL Erlenmeyer flask containing 20 mL of benzene and 1 mL of indicator solution was added. For the preparation of the indicator solution 128 mg of bromothymol blue was dissolved in 100 mL of benzene. The indicator solution has yellow colour and after reaction with solution with catalyst (with basic property) it turned into green colour. Thereafter, the 0.0025–0.001 M benzoic acid in benzene was added dropwise from burette until disappearance of the green colour of the solid particle disappear and solution turned into yellow colour [18]. This titration was repeated at least 3 times. The basicity calculation was presented in mmol/g calculated from the titre of benzoic acid required for the amount of solid sample [14]. The basicity of catalysts was calculated in mmol/g using the following equation:

$$\text{Basicity}\left(\frac{\text{mmol}}{\text{g}}\right) = \frac{\text{Concentration of the titrant solution}\left(\frac{\text{mol}}{\text{L}}\right) \times \text{Volume of the titrant required(mL)}}{\text{Catalyst weight(g)}}$$

2.3. Catalytic evaluation

The scheme of the reactor used for the conversion of glycerol aqueous solution is shown in our previous papers [7,14]. Briefly, the reaction was conducted in the packed-bed microactivity reactor (Microactivity-Reference, PID Eng&Tech). The reactor temperature was set up at 350 °C. Typically, 0.5 g of the powdered catalyst was loaded into a packed bed tubular reactor and stabilized with glass wool on both sides. Glycerol water solutions were kept at room temperature in a reservoir tank outside of the hot box and was injected into the hot box by a 307 HPLC Piston Pump (Gilson Inc.). The feedstock mixture was entering into the hot box with the constant temperature of 140 °C. The temperature of the mixture was achieved with the help of an electric convection heater, controlled by the temperature controller, TIC. The catalytic packed-bed reactor was pre-treated in N_2 (20 mL/min, Messer,

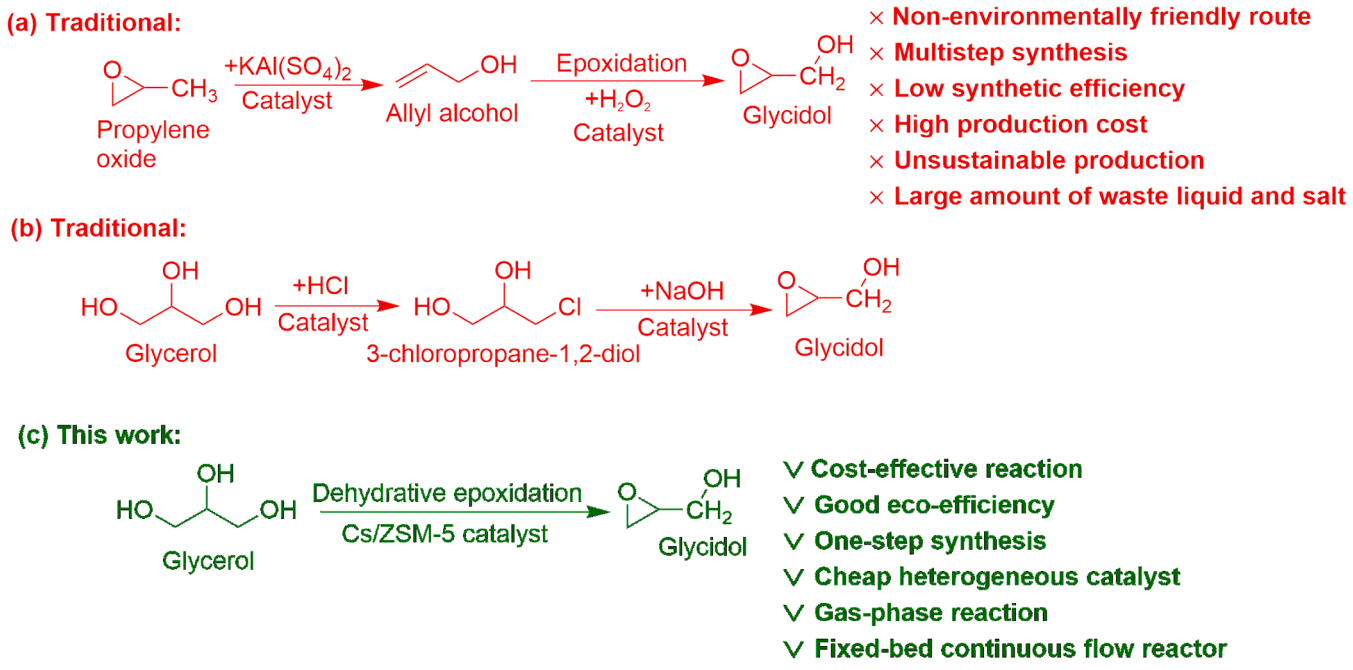

Scheme 1. Traditional and current processes of the glycidol production.

purity 5.0) overnight at 350—500 °C before starting the reaction. Afterward, glycerol was mixed with N_2 and introduced into the packed-bed reactor. The reaction products from the reactor were directed to the Peltier cell and cooled down to 0 °C. Finally, the liquid product was redirected to an additional condenser, which was installed below the reactor.

The collected liquid samples were then analyzed off-line by a gas chromatography GC-FID (Thermo Fisher Scientific, Waltham, MA, USA) with capillary column DB-WAX Ultra Inert (30 m × 0.25 mm × 0.25 μm). All main products were quantified via an external calibration method and verified by a gas chromatography-mass spectrometry system GC-MS (Agilent 7890 A, MS 5977B MSD) with the same capillary column DB-WAX Ultra Inert. Calibration curves were measured in the 0.1–60 wt% range by using chemicals mentioned above in the chemical used paragraph.

The main detected liquid products were glycidol, hydroxyacetone and 1,2-propanediol. The liquid byproduct traces identified by GC-MS were as follows: allyl alcohol, acetaldehyde, acrolein, acetic acid, propionic acid. The online Fusion Inficon micro-GC with Rt-Molsieve 5 A, Rt-Q-BOND, and Rt-U-BOND capillary columns was utilized for qualitative and quantitative analysis of obtained gas product mixture. The relative errors of measured product concentrations were below 5 %. The detected gaseous products were only traces of CO and CO_2.

The total conversion of glycerol conversion, X_{GL}, was calculated using the next equation:

$$X_{GL}(\%) = \frac{n(glycerol)_{in} - n(glycerol)_{out}}{n(glycerol)_{in}} \times 100 \quad (1)$$

where $n(glycerol)_{in}$ and $n(glycerol)_{out}$ are the input and output moles of glycerol before and after the reaction, respectively.

The carbon product selectivity, $S(C_i)$, was calculated using the equation below:

$$S(C_i)(\%) = \frac{mol(P_i) \times C_n}{\sum mol(P_i) \times C_n} \times 100 \quad (2)$$

Carbon yield was calculated on a carbon basis according to the following equation:

$$Y(C_i)(\%) = \frac{mol(P_i) \times C_n}{n(glycerol)_{in} \times C_n} \times 100 \quad (3)$$

Accordingly, the carbon yield can also be expressed as:

$$Y(C_i)(\%) = \frac{X_{GL}}{100} \times S(C_i) \quad (4)$$

$n(P_i)$ and C_n are specified carbon product and carbon number, respectively. The values in this article are in carbon percent. The total mass balance was always higher than 90 % excluding first 2 h TOS. The STY was calculated as following Eq. (3), where the n_i represents the number moles of product, m_{cat} represents the mass of catalysts (g), t represents the reaction time (h).

$$STY\left(mmol \bullet g_{cat}^{-1} \bullet h^{-1}\right) = \frac{n_i}{(m_{cat} \bullet t)} \bullet 1000 \quad (5)$$

Gas hourly space velocity (GHSV) was calculated as follow, where FR is the volumetric flow rate of the gas mixture of N_2 and glycerol at STP, mL/h; and V_{cat} is the volume of the catalyst bed, mL.

$$GHSV_{total}\ \left(h^{-1}\right) = \frac{FR(mL/h)}{V_{cat}(mL)} \quad (6)$$

3. Results and discussion

3.1. Catalyst characterizations

The physicochemical properties of the *x*Cs/ZSM-5 catalysts are summarized in Table 1. Increasing Cs loading had a pronounced impact on surface area, porosity, and crystallinity, which in turn affected the catalytic behavior. ICP-MS results confirmed progressive Cs incorporation from 3.7 wt% to 23.9 wt% for the 5–30 wt% Cs-loaded samples, with notable retention efficiency during wet impregnation. The parent H-ZSM-5 catalyst displayed a high BET surface area (319 m^2/g), which significantly declined upon Cs loading. Particularly, 15Cs/ZSM-5 showed a sharp drop to 66 m^2/g, while 25Cs/ZSM-5 had nearly collapsed porosity (1.9 m^2/g), indicating excessive pore blockage at higher Cs content. Interestingly, while both surface area and micropore volume (V_{micro}) decreased monotonically with Cs content, the mesopore surface area (S_{meso}) and volume (V_{meso}) exhibited a maximum at 5–10 wt% Cs, followed by a rapid decline. At very high Cs loadings (≥25 wt%), $CsNO_3$ deposition reaches a saturation point inside the zeolite pore system. Beyond this threshold, excess $CsNO_3$ preferentially segregates and crystallizes on the external surface, partially relieving pore blockage. As a result, the 30Cs/ZSM-5 sample exhibits a higher BET surface area and micropore volume compared to 25Cs/ZSM-5, despite their similar total Cs contents. BET measurements for both samples were repeated several times, and the results were fully reproducible, supporting the validity of these observations.

Although both 25Cs/ZSM-5 and 30Cs/ZSM-5 were prepared using identical impregnation and calcination procedures, their textural properties differ markedly. ICP-MS confirmed consistent Cs incorporation across the series, excluding variations in loading efficiency as the cause of these differences. The extremely low BET surface area of 25Cs/ZSM-5 (1.9 m^2/g) indicates extensive pore blockage by $CsNO_3$ deposited within the micropore network. In contrast, 30Cs/ZSM-5 shows a partial recovery of porosity, with a BET surface area of 115 m^2/g. This reversal is most plausibly attributed to the redistribution of excess $CsNO_3$ during calcination and the formation of external Cs-rich crystalline domains, as evidenced by HRSEM (Fig. 4**d**) and the sharp $CsNO_3$ reflections in XRD (Fig. 3). Such surface segregation relieves internal pore obstruction and explains the apparent increase in measured porosity of the 30Cs sample despite the similar overall Cs content. The strongest attenuation of MFI peak intensities is observed for 25Cs, consistent with extensive internal occlusion by $CsNO_3$, which enhances X-ray microabsorption and induces

Table 1
Cesium content and structural properties of the *x*Cs/ZSM-5 catalysts.

Catalyst	$Cs^{theor.}$ (wt%)	Cs^a (wt%)	S^b_{BET} (m^2/g)	S^b_{micro} (m^2/g)	S^b_{meso} (m^2/g)	V^c_{micro} (cm^3/g)	V^c_{total} (cm^3/g)	V^c_{meso} (cm^3/g)	PD^d (nm)	HF^e	Crystallite size^f (nm)	Crystallinity^f (%)
H-ZSM-5	–	–	319	261	58	0.141	0.184	0.043	3.5	0.139	68.6	100
5Cs/ZSM-5	5.0	3.7	295	157	138	0.090	0.176	0.086	3.0	0.239	67.5	84.6
10Cs/ZSM-5	10.0	10.8	227	147	80	0.072	0.129	0.057	3.2	0.197	68.9	47.0
15Cs/ZSM-5	15.0	16.0	66	47	19	0.025	0.043	0.018	3.9	0.167	68.7	33.9
20Cs/ZSM-5	20.0	17.2	97	68	29	0.034	0.059	0.025	3.7	0.172	65.1	38.4
25Cs/ZSM-5	25.0	22.0	1.9	3.4	1.5	–	–	–	–	–	62.5	19.8
30Cs/ZSM-5	30.0	23.9	115	91	24	0.046	0.068	0.022	3.5	0.141	65.9	33.2

[a]ICP-MS. [b]BET method. [c]t-plot method. [d]Average pore diameter measured from the desorption branch according to the BJH method. [e]Hierarchy factor (HF) = (S_{meso}/S_{BET})× (V_{micro}/V_{total}). [f]The crystallite size and crystallinity were obtained from XRD data.

local disorder within the zeolite crystals, thereby lowering the apparent framework intensity without indicating structural collapse. In contrast, 30Cs exhibits the most intense $CsNO_3$ reflections together with a smaller relative reduction of MFI peak intensity, indicating that excess $CsNO_3$ segregates toward the external surface during calcination, forming crystalline domains that partially relieve internal pore blockage. This interpretation is fully consistent with the partial BET surface area recovery observed for the 30Cs sample.

The 15Cs/ZSM-5 sample retained modest mesoporosity (S_{meso} = 19 m^2/g; V_{meso} = 0.018 cm^3/g), suggesting an optimal balance between mesostructure preservation and active site generation. This balance is reflected in the hierarchy factor (HF), which peaked at 5Cs/ZSM-5 (0.239), then declined steadily with increasing Cs content. However, the catalyst with the highest glycidol selectivity and STY of 15Cs/ZSM-5 showed a moderate HF (0.167), indicating that maximal hierarchical porosity is not the only descriptor of catalytic performance. Instead, it is likely that 15Cs achieves an optimal surface chemical environment, with sufficient base site concentration, acceptable crystallinity (33.9 %), and accessible mesopores facilitating the tandem dehydration-epoxidation sequence leading to glycidol. Additionally, crystallite size analysis from XRD indicates slight structural contraction at high Cs content, although no major framework collapse occurred. The reduction in crystallinity from 100 % (H-ZSM-5) to 19.8 % (25Cs/ZSM-5) further supports partial disruption of the long-range order, possibly contributing to the formation of catalytically active defect sites or partially amorphous domains with enhanced basic functionality.

The N_2 adsorption-desorption isotherms (Fig. 2**a**) of the *x*Cs/ZSM-5 catalysts reveal a clear dependence of surface area and porosity on Cs loading. The parent H-ZSM-5 exhibited the highest adsorption capacity, consistent with its unmodified microporous structure. Upon $CsNO_3$ impregnation, a gradual reduction in total adsorbed volume was observed, indicating partial pore blockage and decreased surface area, which intensified with increasing Cs content from 5 to 30 wt%. Notably, the 5Cs/ZSM-5 sample retained a comparatively high adsorbed volume relative to other Cs-modified catalysts, suggesting an optimal balance between Cs incorporation and textural accessibility.

The BJH pore size distribution profiles (Fig. 2**b**) and corresponding average pore diameters (PD) listed in Table 1 offer important insights into the structural evolution of ZSM-5 upon Cs modification. The parent H-ZSM-5 shows a relatively narrow mesopore distribution centered around 25–30 Å with an average pore diameter of 3.5 nm, characteristic of typical microporous-mesoporous transition behavior due to intercrystalline voids or slight framework defects. Upon Cs impregnation, the pore size distribution broadens for low Cs loadings (5–10 wt%), particularly in the 20–50 Å range, suggesting the emergence of additional mesoporosity. This is likely attributed to partial restructuring during thermal treatment and the introduction of Cs salt particles that create interparticle voids [7,19]. The average PD remained relatively stable across all catalysts, ranging between 3.0 and 3.9 nm. While 5Cs/ZSM-5 exhibited a slightly smaller PD (3.0 nm), the 15Cs/ZSM-5 catalyst showed the highest PD of 3.9 nm, despite having a much lower total surface area. This increase in pore diameter suggests the development of wider mesopores, which likely contributed to its superior catalytic performance by mitigating internal diffusion limitations and reducing residence time for glycidol, a moderately bulky epoxide prone to secondary reactions. At higher Cs contents (≥20 wt%), both mesopore volume and PD slightly decreased, accompanied by a dramatic loss of total surface area and mesoporous fraction. This trend indicates that excessive Cs loading leads to pore blockage or partial collapse of the hierarchical framework due to salt aggregation and densification during calcination. Such structural densification likely contributes to the lower observed catalytic activity at high Cs loadings, despite comparable Cs content on the surface. While mesoporosity decreases progressively up to 25Cs due to pore blocking, at 30Cs the mesopore volume becomes comparable to that of the 20Cs sample. This can be attributed to redistribution of Cs species and their preferential accumulation on the external surface at higher loadings, which reduces the extent of internal pore occlusion and leads to a non-linear trend in mesoporosity. Thus, the optimal balance between accessible mesopores (20–50 Å), high PD (~3.9 nm), and Cs incorporation in the 15Cs/ZSM-5 catalyst suggests that not only the quantity but also the quality and distribution of mesoporosity play a vital role in determining glycidol selectivity and STY. This reinforces the importance of fine-tuning alkali loading to retain hierarchical features without excessive structural degradation.

The XRD patterns presented in Fig. 3 and Fig. S1 reveal the structural transformations occurring upon impregnation of H-ZSM-5 with different amounts of $CsNO_3$. In the parent H-ZSM-5 sample, sharp and well-defined reflections between 7° and 9°, and in the range of 22–25° (Fig. 3**a**), are consistent with the highly crystalline MFI framework structure. These characteristic peaks remain visible in all Cs-modified samples, indicating that the zeolite long-range order is largely retained after $CsNO_3$ deposition, even at higher loadings. However, notable changes in peak intensities and the appearance of additional reflections provide deeper insights. The $CsNO_3$-related peaks, marked with triangles (Δ) and identified from the Crystallography Open

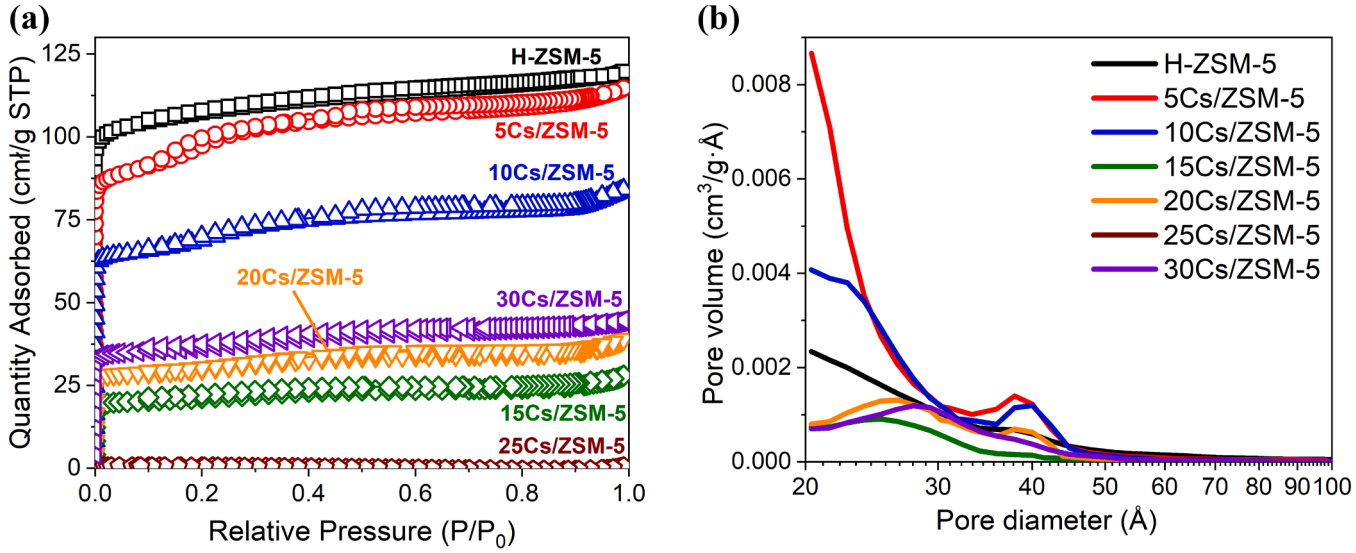

Fig. 2. N_2 adsorption-desorption isotherms – (a) and BJH pore size distribution – (b) of the *x*Cs/ZSM-5 and H-ZSM-5 catalysts.

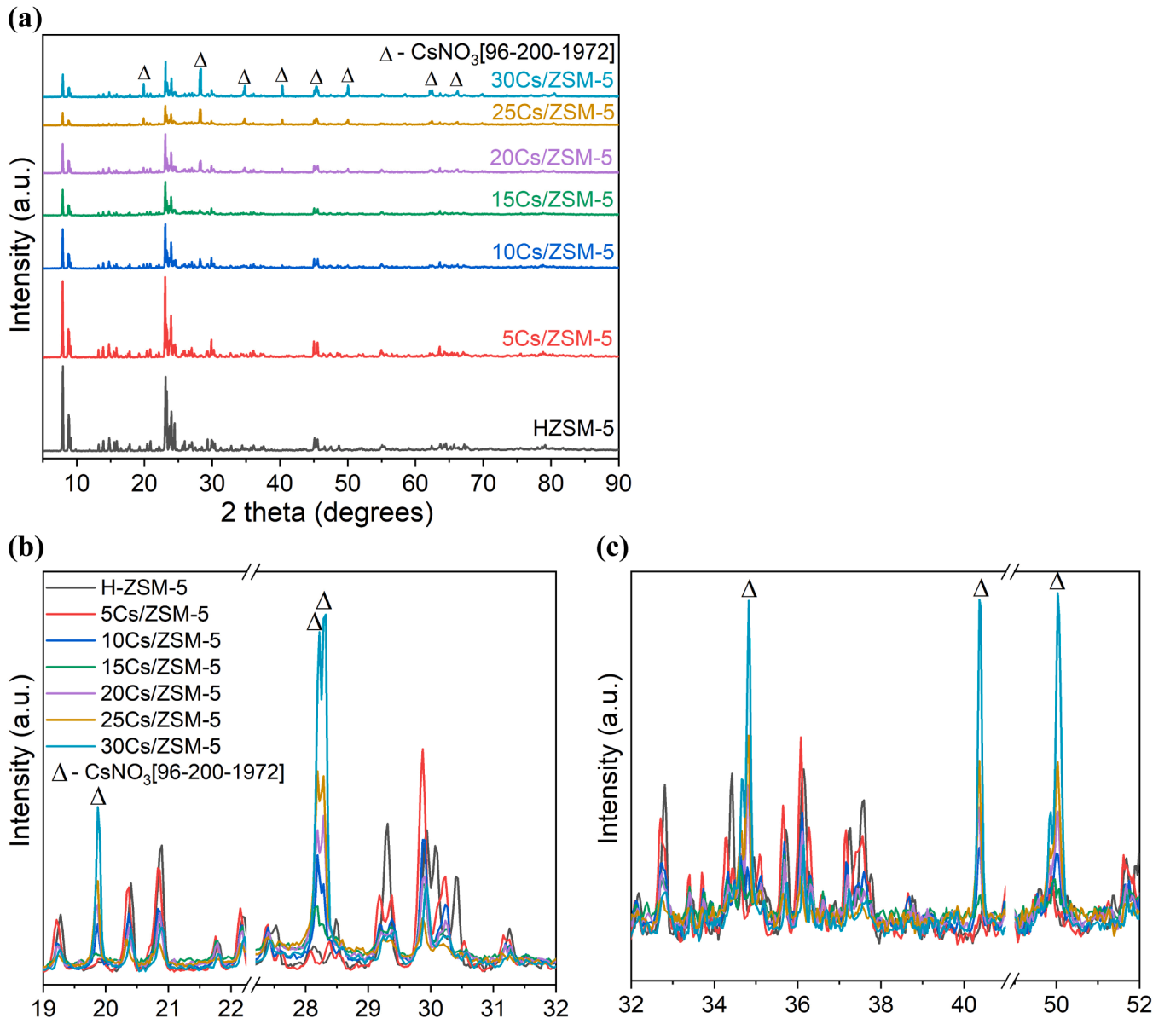

Fig. 3. (a) – XRD patterns of the H-ZSM-5 and *x*Cs/ZSM-5 catalysts, (b) – close up of the 19–22.3° and 27.2–32° ranges and (c) – close up of the 32–41° and 49–52° 2 theta ranges. The diffraction lines of $CsNO_3$ were derived from the COD database [96–200–1972].

Database (COD #96–200–1972), begin to emerge in the 10Cs/ZSM-5 pattern and intensify progressively with increasing Cs content. This trend is particularly evident in the enlarged regions of Fig. 3**b** (19–22.3° and 27.2–32°) and Fig. 3**c** (32–41° and 49–52°), where distinct $CsNO_3$ reflections at $2\theta = 28.3°$, 34.9°, 40.4°, and 50.1° become dominant in the 25Cs/ZSM-5 and 30Cs/ZSM-5 samples.

The absence of $CsNO_3$ peaks in 5Cs/ZSM-5 suggests high dispersion or amorphous deposition of the cesium nitrate at low loading. As the loading increases, crystalline $CsNO_3$ domains form and grow, reflecting reduced dispersion and possibly partial phase segregation on the zeolite surface. This trend is accompanied by a systematic attenuation of the MFI zeolite peaks, suggesting that $CsNO_3$ deposition may partially block the pore system or attenuate the X-ray signal from the underlying zeolite due to surface coverage. Furthermore, the increased crystallinity of $CsNO_3$ at higher loadings implies reduced interaction between Cs species and the zeolite framework, which may affect catalyst performance. For example, moderate loading (e.g., 15Cs/ZSM-5) may offer an optimal balance between basic site availability and textural integrity, whereas excessive $CsNO_3$ crystallization in 25–30Cs/ZSM-5 may block active sites or hinder reactant diffusion.

Although no significant shifts were observed in the main MFI diffraction peaks across the Cs-modified samples, this does not entirely rule out partial ion exchange or local structural alterations, especially at higher $CsNO_3$ loadings. The preservation of peak positions suggests that the long-range order of the zeolite framework remains largely intact. However, it is well documented in the literature [15] that alkali metals (Rb and Cs) can chemically interact with siliceous frameworks, potentially disrupting the local structure and even leading to the degradation of ordered mesoporous architectures. In the context of ZSM-5, such interactions may result in partial framework dealumination, neutralization of Brønsted acid sites, or the formation of extra-framework species. Furthermore, the increasing intensity of $CsNO_3$ reflections and the concurrent decrease in MFI peak intensity at high Cs loadings indicate substantial surface deposition, pore blockage, and possibly partial loss of microporosity. While the $CsNO_3$ peak intensities increase steadily with Cs loading, the MFI reflections display a less regular trend. This non-linear behavior can be attributed to a combination of factors, including attenuation of X-ray signals by heavy Cs species, partial pore

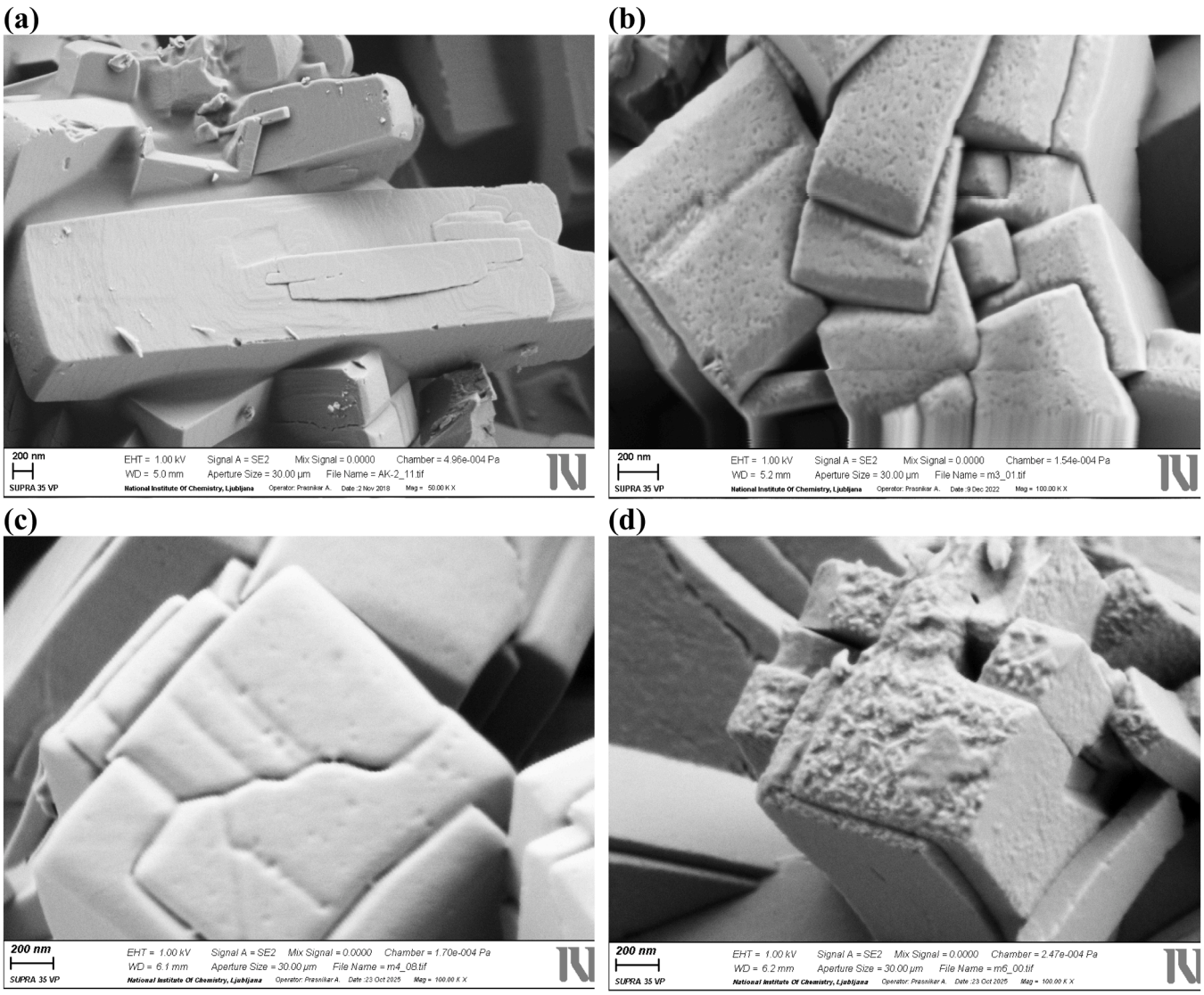

Fig. 4. HRSEM images of the H-ZSM-5 catalyst (a) and Cs-modified ZSM-5 catalysts with different Cs loadings: 15Cs/ZSM-5 (b), 25Cs/ZSM-5 (c), and 30Cs/ZSM-5 (d).

filling and occlusion, and changes in crystallite/domain size and preferred orientation at high loadings. These effects modify the apparent MFI peak intensities without indicating structural collapse. The trend correlates with the micropore surface area and volume data in Table 1, reflecting changes in structural accessibility rather than framework degradation.

The HRSEM images (Fig. 4) reveal clear morphological differences between the unmodified H-ZSM-5 and the optimized 15Cs/ZSM-5 catalyst, which correlate well with the observed textural and catalytic trends. The pristine H-ZSM-5 (Fig. 4**a**) displays typical coffin-shaped crystals with smooth and well-faceted surfaces, indicative of high crystallinity and the preserved MFI zeolite framework. The absence of visible defects and the dense packing of crystals suggest limited mesoporosity and minimal surface irregularities. In contrast, the surface morphology of 15Cs/ZSM-5 (Fig. 4**b**) appears significantly roughened and textured, with numerous surface depressions and voids resembling a sponge-like structure. This structural transformation likely stems from localized framework distortion or partial amorphization induced by $CsNO_3$ impregnation and subsequent calcination. The emergence of surface pits and intergranular voids in 15Cs/ZSM-5 may contribute significantly to the observed increase in average pore diameter (3.9 nm). These surface modifications are advantageous for catalytic performance, as they facilitate improved glycerol diffusion and desorption of bulky intermediates such as glycidol. Moreover, the increased surface roughness and defect density may expose additional active sites or alter the acid-base properties of the external surface, promoting the desired tandem dehydration-epoxidation reaction. Altogether, SEM observations support the conclusion that moderate Cs modification (as in 15Cs/ZSM-5) induces beneficial morphological changes without collapsing the zeolite framework, thereby contributing to the enhanced selectivity and STY of glycidol. It is worth noting that the relatively large crystal size of the ZSM-5 zeolite support may contribute to faster coke deposition and catalyst deactivation due to longer diffusion pathways and lower external surface area. The use of nano-sized ZSM-5 could enhance mass transport and potentially improve catalyst stability. This aspect will be explored in future studies, where different zeolite crystal sizes will be compared to further optimize catalyst performance.

To better understand the morphological changes induced by high $CsNO_3$ loading, additional HRSEM analyses were performed for 25Cs/ZSM-5 and 30Cs/ZSM-5 catalysts (Fig. 4**c-d**). In contrast to the smooth and well-faceted surface of the parent H-ZSM-5 (Fig. 4**a**) and the moderately roughened texture of 15Cs/ZSM-5 (Fig. 4**b**), the 25Cs and 30Cs samples exhibit pronounced surface irregularities, densification, and partial coverage by $CsNO_3$ agglomerates. This indicates that a

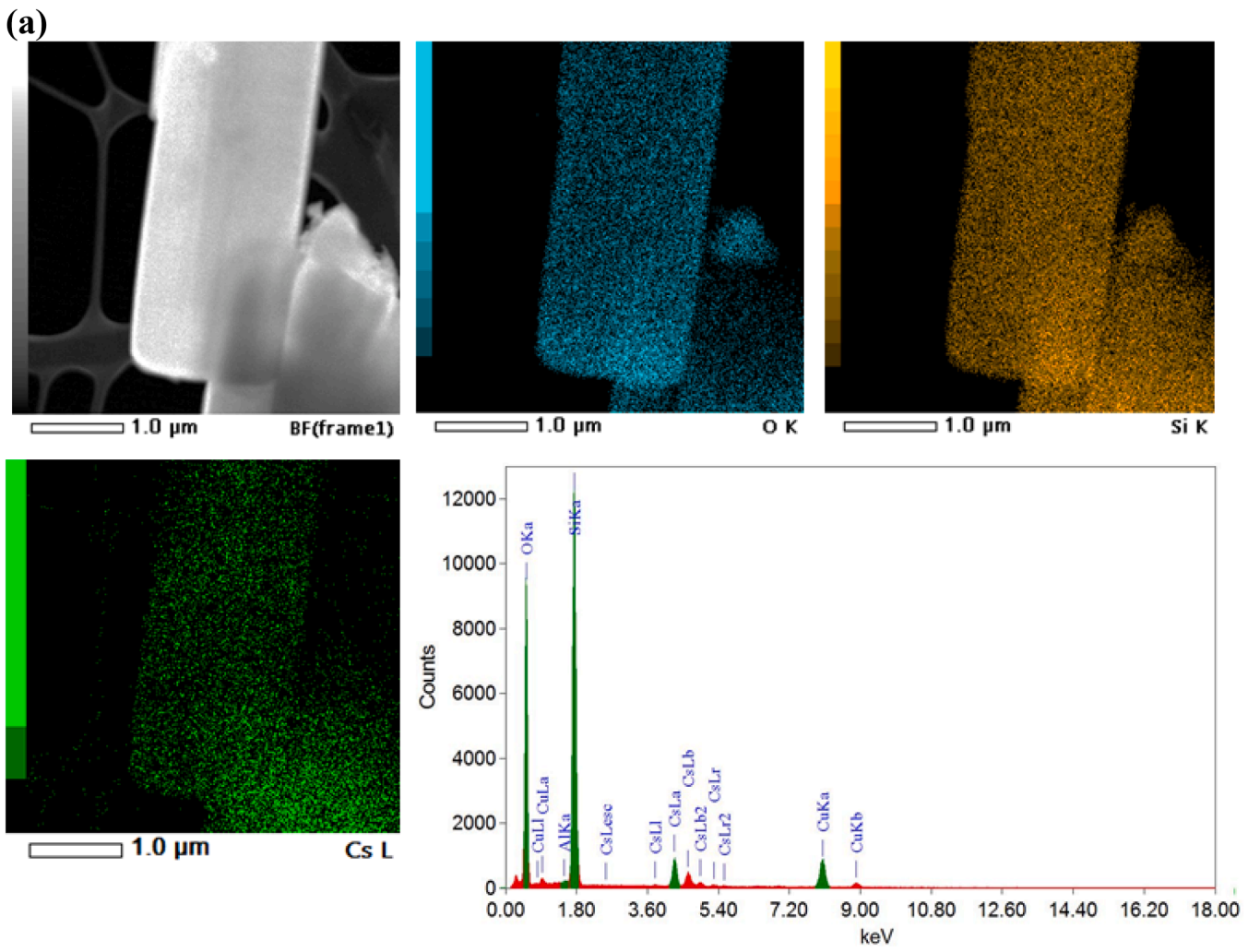

Fig. 5. STEM-HAADF image and elemental mapping of the 15Cs/ZSM-5 catalyst – (a), and surface basicity of the *x*Cs/ZSM-5 catalysts – (b).

considerable portion of $CsNO_3$ remains on the external surface even after calcination. The morphological distortion becomes more severe at 30Cs, where extensive $CsNO_3$ crystallization, surface disorder, and clear signs of amorphization of the zeolite framework are observed. These structural modifications correlate with the attenuation of MFI reflections in XRD and the strong decline in textural properties. Overall, excessive $CsNO_3$ loading leads to surface agglomeration, pore blocking, and partial framework degradation, which explain the reduced catalytic performance of these materials at high Cs contents.

STEM-HAADF imaging combined with EDX elemental mapping (Fig. 5**a**) was performed to evaluate the spatial distribution of Cs species on the surface of the optimized 15Cs/ZSM-5 catalyst. The bright-field image shows well-defined zeolite crystallites with sharp edges and uniform contrast, suggesting retention of the overall MFI crystal morphology after Cs modification. Elemental maps of oxygen (O K), silicon (Si K), and cesium (Cs L) reveal a homogeneous distribution of the framework elements (Si, O), as expected for ZSM-5. Importantly, Cs is also uniformly dispersed across the entire zeolite crystallite surface, with no visible agglomeration or phase separation. This suggests efficient anchoring of Cs^+ species onto the external surface and possibly into near-surface exchange or defect sites during wet impregnation and calcination.

The Cs signal is sufficiently intense and evenly distributed, indicating that the theoretical loading of 15 wt% (and 16 wt% by ICP-MS) resulted in well-dispersed Cs species rather than bulk salt domains. Such uniformity in Cs dispersion is essential for generating consistent surface basicity, which plays a critical role in facilitating the tandem dehydration-epoxidation mechanism leading to glycidol. Additionally, the absence of Cs-rich clusters supports the observed stability of the catalyst over extended TOS, as large salt domains are more prone to sintering and deactivation. The corresponding EDX spectrum confirms the presence of Cs, Si, and O without detectable impurity phases, reinforcing the high purity and controlled modification of the catalyst surface. The STEM-EDX analysis demonstrates that 15Cs/ZSM-5 possesses a well-preserved crystalline framework with homogeneously distributed Cs, supporting its outstanding catalytic performance in the one-step gas-phase production of glycidol under ambient pressure.

The surface basicity of the *x*Cs/ZSM-5 catalysts, determined by

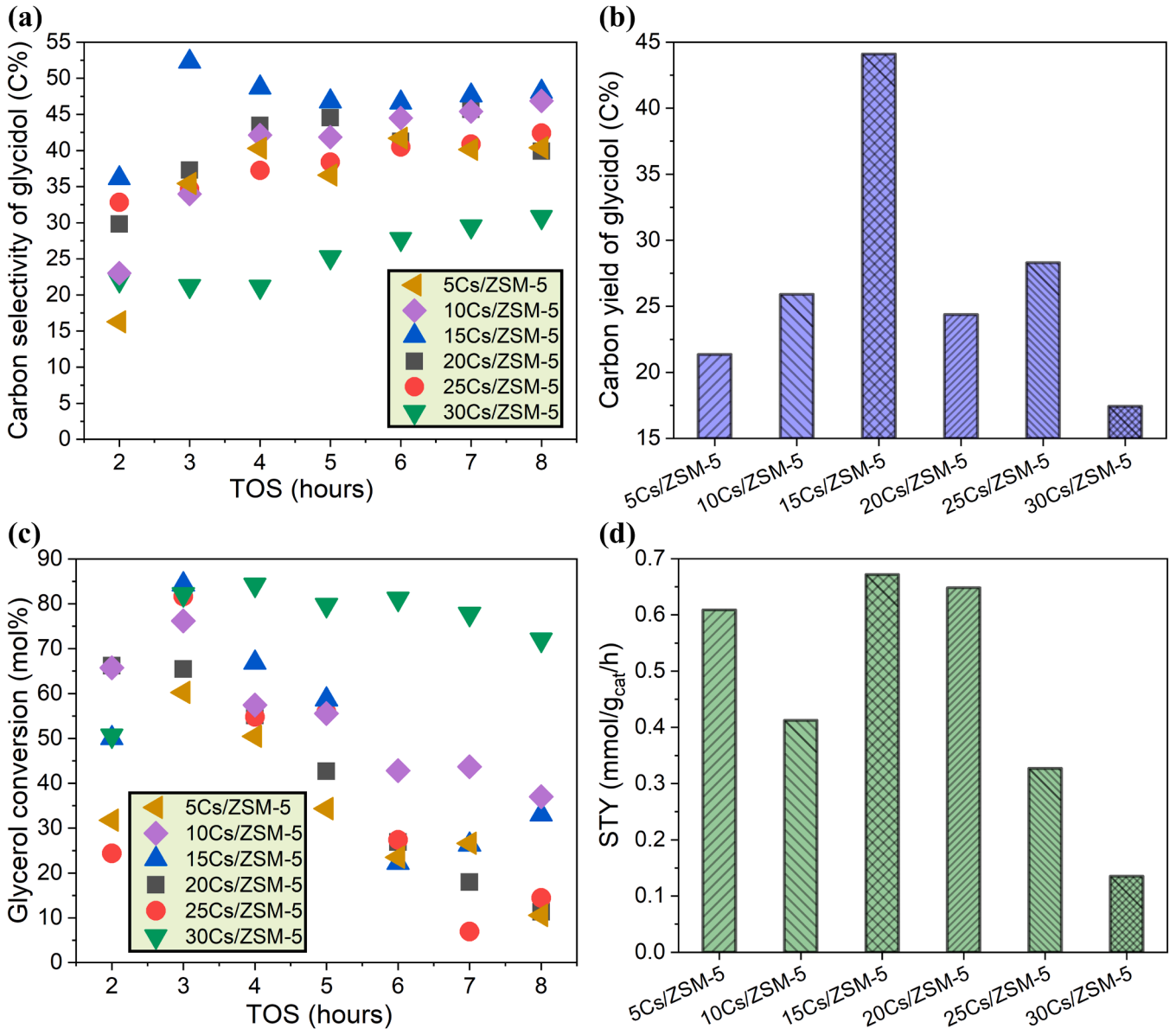

Fig. 6. The effect of $CsNO_3$ loading on the glycidol selectivity — (a), glycidol yield — (b), glycerol conversion — (c), and STY — (d). Reaction conditions: catalyst, 0.5 g; $T_{reactor}$ = 350 °C; P = 1 bar; C(GL) = 10 wt%; FR(N_2) = 20 mL/min; FR(GL) = 2.34 mL/h; $GHSV_{total}$ = 968 h^{-1}.

benzoic acid titration using bromothymol blue as a Hammett indicator (Fig. 5**b**), provides crucial insight into the catalytic behavior of the series. The basicity trend follows the order: 30Cs > 15Cs > 10Cs > 25Cs > 20Cs > 5Cs, indicating that surface basicity does not increase linearly with Cs loading. Instead, it reflects a complex interplay between Cs dispersion, accessibility of surface sites, and pore structure. The 15Cs/ZSM5 catalyst, which demonstrated the highest glycidol selectivity and STY, exhibited moderately high basicity, suggesting that an optimal level of surface basicity, rather than the maximum, is most beneficial for selective glycidol formation. Excessive basicity, as observed for 30Cs/ZSM-5, may lead to side reactions, catalyst fouling, or destabilization of the glycidol product, while insufficient basicity (5Cs/ZSM-5) limits glycerol activation and epoxide ring closure.

The non-monotonic relationship between Cs loading and basicity can be rationalized by two competing effects: (i) the generation of new basic sites associated with dispersed Cs^+ species and (ii) partial pore blockage and surface agglomeration at higher loadings, which can shield or deactivate these sites. Although this explanation is consistent with the observed basicity trends and HRSEM data (Fig. 4), it remains a plausible interpretation rather than direct experimental proof. Elemental mapping of the 15Cs/ZSM-5 catalyst (Fig. 5**a**) confirms homogeneous Cs distribution at optimal loading. At higher $CsNO_3$ contents (≥20 wt%), the increased surface roughening and $CsNO_3$ agglomeration observed by HRSEM suggest reduced accessibility of basic sites, which correlates with the lower measured basicity for 25Cs/ZSM-5 and 30Cs/ZSM-5. These observations confirm that basic site density and accessibility, rather than Cs content alone, govern the catalytic performance. The excellent activity of 15Cs/ZSM-5 can be ascribed to its ideal combination of well-dispersed and accessible basic sites, maintained porosity, and moderate crystallinity, creating a catalytic surface environment conducive to tandem glycerol dehydration and intramolecular epoxidation under mild conditions.

3.2. Catalytic performance

3.2.1. The effect of $CsNO_3$ loading

The catalytic performance of *x*Cs/ZSM-5 catalysts in the one-step gas-phase conversion of glycerol to glycidol was strongly influenced by Cs loading, as shown in Fig. 6. The full datasets underlying Figs. 6–16 are listed in Tables S1-S18 (**Support Information file**), including operating conditions and the corresponding values of X_{GL}, S_i (C%), $Y_{glycidol}$ (C%), and mass balance. All experiments were conducted under ambient pressure using 10 wt% glycerol feed at 350 °C. The carbon selectivity of glycidol (Fig. 6**a**) showed a clear maximum for the 15Cs/ZSM-5 catalyst, maintaining high values (up to 54 %) throughout the 8 h TOS, with remarkable stability. In contrast, both low (5Cs/ZSM-5) and high Cs loadings (≥25 wt%) exhibited reduced selectivity, likely due to insufficient basicity in the former and pore blockage or excessive basicity in the latter. The lower catalytic performance of 30Cs/ZSM-5 does not originate solely from lower porosity. In fact, its mesopore volume and surface area are slightly higher than those of the 15Cs sample (Table 1). Rather, the reduced activity is primarily attributed to extensive $CsNO_3$ agglomeration on the external surface (Fig. 4**d**), which likely decreases the effective accessibility of active basic sites. Such agglomeration can also induce local mass-transfer limitations, accelerate catalyst fouling, and increase the probability of glycidol overconversion, thereby explaining the inferior catalytic performance of the 30Cs catalyst despite its higher nominal mesoporosity.

Importantly, as shown in Fig. 6**b**, 15Cs/ZSM-5 also exhibited the highest carbon yield of glycidol (~44 C%), outperforming all other Cs loadings. This high yield reflects an optimal synergy between conversion and selectivity, making 15Cs/ZSM-5 the most efficient catalyst under the tested conditions. The glycerol conversion data (Fig. 6**c**) show that 30Cs/ZSM-5 achieved the highest initial conversion (>85 %) and maintained values above 70 % during TOS = 3–8 h. However, its low selectivity and $CsNO_3$ agglomeration make it less attractive despite the high activity. In contrast, 15Cs/ZSM-5 provided a moderate but stable conversion (~35–85 %) and superior selectivity, confirming that high glycidol yield can be achieved without maximizing glycerol conversion when the reaction pathway is efficiently directed toward the epoxide product. The STY results (Fig. 6**d**) further support the outstanding performance of 15Cs/ZSM-5, with the highest STY value of ~0.67 $mmol \cdot g_{cat}^{-1} \cdot h^{-1}$. This result clearly demonstrates that glycidol production under mild, continuous-flow conditions is maximized not by extreme Cs loadings or surface basicity alone, but by achieving the right balance between porosity, surface functionality, and active site accessibility.

The gradual decrease in glycerol conversion with increasing TOS is attributed to progressive catalyst deactivation during continuous gas-phase operation at elevated temperature. Three main factors contribute to this behavior: (i) coke deposition resulting from secondary condensation and polymerization of glycerol-derived intermediates, leading to pore blockage and reduced accessibility of active sites; (ii) thermal redistribution and partial sintering of Cs species, which decreases the number of well-dispersed basic sites responsible for intramolecular epoxidation; and (iii) structural rearrangements of the zeolite framework accompanied by a partial loss of surface area, which negatively affect both the acidity and basicity of the catalyst.

Based on our previous studies (Fig. S2), post-reaction XRD analysis of spent catalysts, compared with the corresponding fresh samples with different Cs loadings (10Cs/ZSM-5 and 20Cs/ZSM-5), revealed decreases in peak intensity and slight peak shifts, indicating Cs redistribution and partial structural modification of the zeolite framework [7]. These structural changes are consistent with the observed deactivation trends. Catalyst deactivation proceeds in two distinct stages: the first stage corresponds to a rapid decline in activity caused by partial decomposition of the $CsNO_3$ active phase, while the second stage involves a slower decrease in performance primarily due to progressive coke accumulation.

For 10Cs/ZSM-5(spent), peak shifts and pronounced intensity decreases were observed, indicating framework damage caused by coke deposition, steam hydrolysis, and Cs-induced attack. For 20Cs/ZSM-5 (spent), $CsNO_3$ decomposition was evident, while the MFI framework remained partially intact. TGA analysis of the spent catalysts (Fig. 13) further confirms the presence of carbonaceous deposits in the temperature range of 300–500 °C, which is characteristic of soft coke formation. This observation correlates well with the decline in glycerol conversion, while glycidol selectivity remains relatively stable during the early reaction stage.

The product selectivity and temporal evolution during the continuous-flow conversion of glycerol over 15Cs/ZSM-5 at 350 °C are shown in Fig. 7**a**. Glycidol remained the dominant product throughout 8 h TOS, with carbon selectivity ranging between 50–55 C%, demonstrating the high chemoselectivity and functional stability of the catalyst. Despite the decline in glycerol conversion from ~82 % (at 3 h) to ~22 % (at 6–8 h), glycidol selectivity remained remarkably stable, suggesting that the active basic sites responsible for epoxidation remain intact, while catalyst deactivation primarily impacts dehydration activity or surface diffusion.

Minor byproducts included hydroxyacetone, 1,2-propanediol, acetaldehyde and small amounts of allyl alcohol and acrolein, indicating competing dehydration and rearrangement reactions. The presence of hydroxyacetone and allyl alcohol in particular suggests a pathway involving initial glycerol dehydration, followed by C–C or C–O rearrangement steps. The low and stable levels of acrolein and other deep-dehydration products point to the ability of 15Cs/ZSM-5 to suppress overconversion and undesired fragmentation reactions, which are typically promoted on excessively basic sites.

The corresponding GC-FID chromatogram (Fig. 7**b**) supports the compositional data, showing a dominant glycidol peak alongside well-separated signals for byproducts such as acetaldehyde, acrolein, propionaldehyde, hydroxyacetone, allyl alcohol, and 1,2-propanediol. The

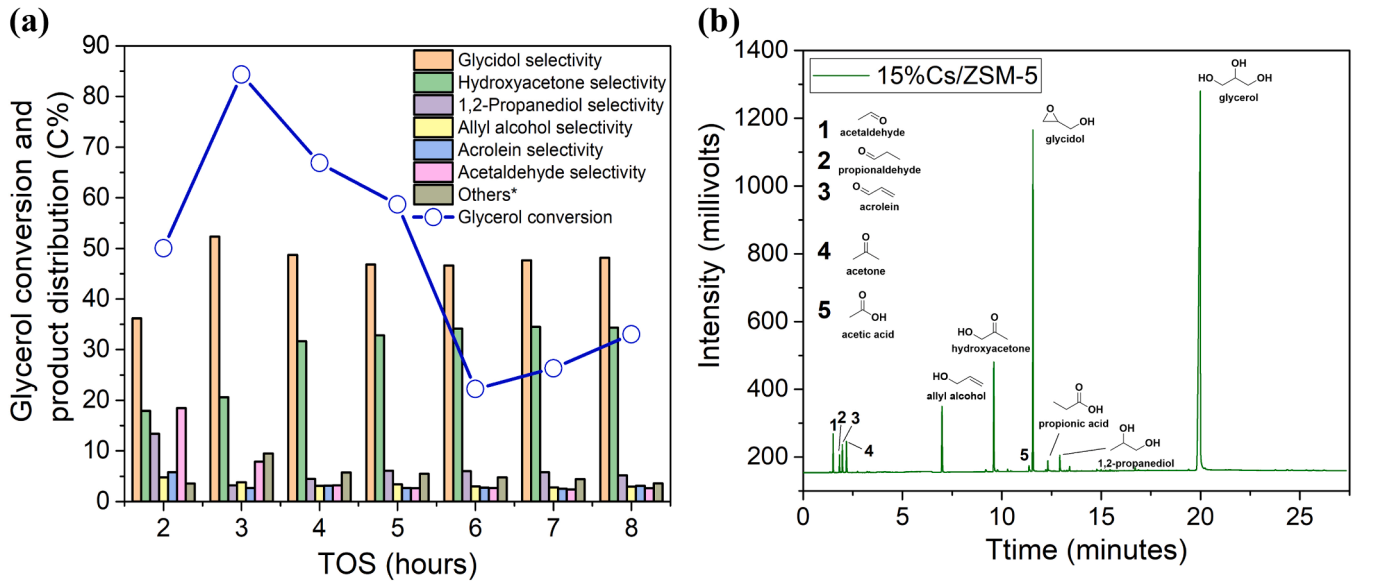

Fig. 7. Product distribution over the 15Cs/ZSM-5 catalyst during 8 h TOS (a); and GC-FID spectrum from a typical run using the 15Cs/ZSM-5 catalyst (b). Reaction conditions: catalyst, 0.5 g; $T_{reactor}$ = 350 °C; P = 1 bar; C(GL) = 10 wt%; FR(N_2) = 20 mL/min; FR(GL) = 2.34 mL/h; $GHSV_{total}$ = 968 h^{-1}.

presence of multiple oxygenates underscores the complexity of the glycerol conversion network, but also confirms the versatility of the Cs-modified zeolite in directing reactivity toward valuable intermediates under mild operating conditions. Taken together, the temporal product analysis and chromatographic profile support a tandem mechanism involving:

- Initial glycerol dehydration, potentially forming hydroxyacetone or enol intermediates.
- Intramolecular epoxidation on surface basic sites to yield glycidol.
- Suppression of polymerization and coke-forming pathways, ensuring clean product distribution.

The observed product spectrum and selectivity pattern further validate that 15Cs/ZSM-5 achieves an ideal balance of surface basicity and pore accessibility, enabling selective transformation of glycerol into glycidol with minimal undesired byproducts, even over prolonged operation.

3.2.2. *The effect of reaction temperature and TOS*

The influence of reaction temperature on glycidol formation was systematically investigated over the 15Cs/ZSM-5 catalyst under standard flow conditions, and the results are presented in Fig. 8. A clear temperature-dependent trend was observed in both carbon selectivity (Fig. 8**a**) and STY (Fig. 8**b**). Raising the temperature from 350 to 450 °C led to a substantial improvement in catalytic performance. Glycidol selectivity increased from ~48 % to a maximum of ~68 %, while STY rose from 0.6 to 1.3 $mmol \cdot g_{cat}^{-1} \cdot h^{-1}$, indicating that elevated temperature enhances both the intrinsic activity and selectivity of the catalyst. This enhancement may be attributed to increased rates of glycerol dehydration and epoxidation, coupled with improved desorption of glycidol from the catalyst surface, minimizing its overreaction.

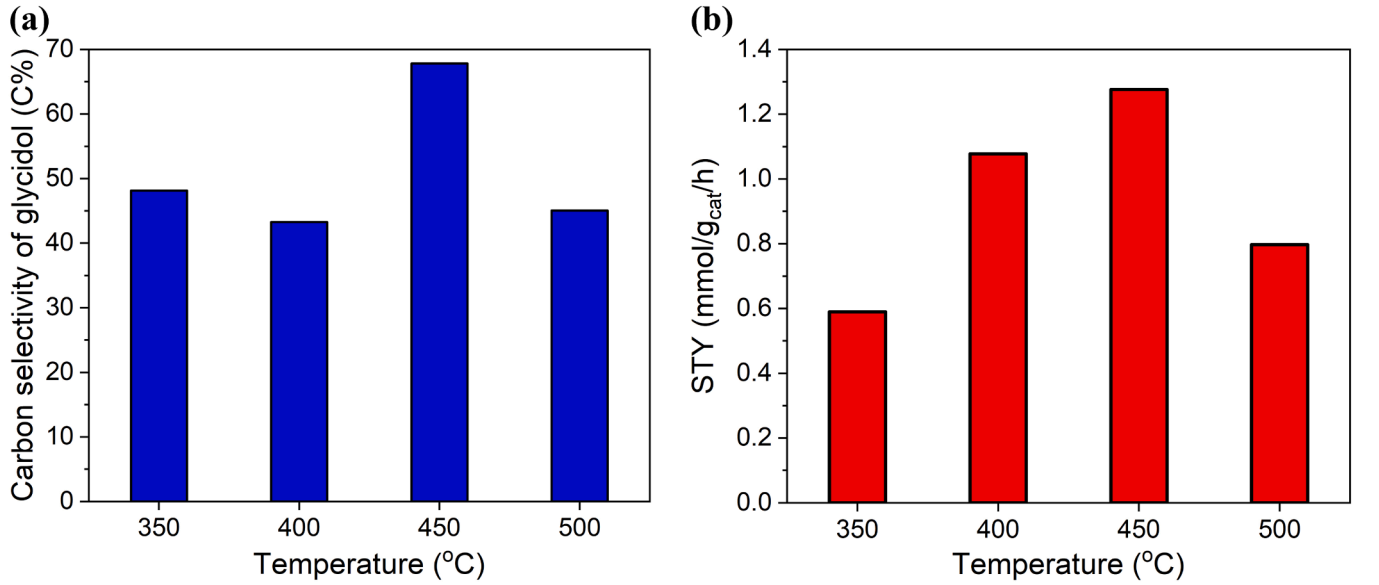

Fig. 8. The effect of reaction temperature on the glycidol selectivity — (a) and STY — (b). Reaction conditions: 15Cs/ZSM-5 catalyst, 0.5 g; TOS = 8 h; C(GL) = 10 wt%; P = 1 bar; FR(N_2) = 20 mL/min; FR(GL) = 2.34 mL/h; $GHSV_{total}$ = 968 h^{-1}.

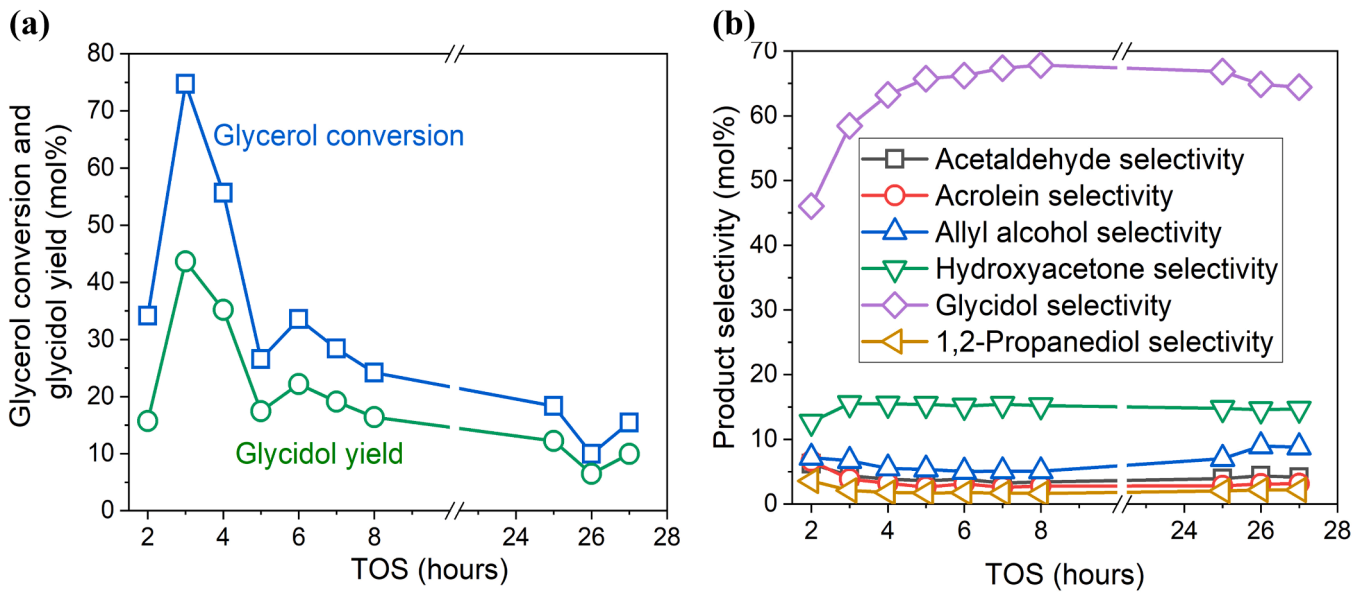

Fig. 9. The effect of TOS on the glycerol conversion and glycidol yield – (a) and product selectivity – (b). Reaction conditions: 15Cs/ZSM-5 catalyst, 0.5 g; $T_{reactor}$ = 450 °C; C(GL) = 10 wt%; FR(N_2) = 20 mL/min; FR(GL) = 2.34 mL/h; $GHSV_{total}$ = 968 h^{-1}; TOS = 27 h.

However, a further increase to 500 °C resulted in a marked decline in both selectivity (~47 %) and STY (~0.8 mmol·g_{cat}^{-1}·h^{-1}). This suggests that excessively high temperatures promote competing pathways such as glycerol cracking, deep dehydration, or even glycidol decomposition, which ultimately reduce the desired product yield and increase carbon loss to unquantified or coke-forming species.

The observed volcano-type dependence indicates that 450 °C is the optimal reaction temperature for maximizing glycidol formation over 15Cs/ZSM-5, striking a balance between kinetic activation and product stability. Operating below this temperature may result in incomplete glycerol activation, while operating above it risks unselective conversion. These results further validate the robustness and versatility of 15Cs/ZSM-5, demonstrating that the catalyst can operate efficiently across a wide temperature range, but with a clear optimum for maximizing productivity and selectivity under continuous-flow, ambient-pressure conditions.

The long-term catalytic stability of 15Cs/ZSM-5 under optimal reaction conditions (450 °C, 1 bar) was evaluated over 27 h of continuous operation, and the results are shown in Fig. 9. The data highlight both the strengths and the limitations of the system under extended exposure to reaction conditions. As shown in Fig. 9**a**, glycerol conversion initially peaked at ~75 % at TOS = 3 h, followed by a gradual decline to ~16 % at TOS = 27 h. The glycidol yield exhibited a similar trend, peaking at ~44 % before decreasing to ~10 % after 27 h. The gradual decline in catalytic activity observed during extended operation can be primarily attributed to coke deposition, as confirmed by TGA of the spent catalysts (Fig. 13), which revealed the presence of both soft and hard coke fractions. Additional factors such as partial Cs phase redistribution and progressive pore obstruction are plausible, supported indirectly by the attenuation of MFI reflections and $CsNO_3$-related peaks in XRD, as well as the surface densification observed by HRSEM at higher Cs loadings [7, 14]. Importantly, the product selectivity remained relatively stable over TOS, indicating that catalyst deactivation in this system predominantly affects activity rather than intrinsic chemoselectivity. Further studies involving *in situ* or post-reaction elemental mapping and porosity analysis would provide a more definitive understanding of these deactivation phenomena.

Indeed, product selectivity trends (Fig. 9**b**) confirm that glycidol remained the dominant product throughout the TOS window, maintaining a high and relatively stable selectivity of ~65–68 %. Minor byproducts such as hydroxyacetone, allyl alcohol, acrolein, acetaldehyde, and 1,2-propanediol were consistently detected in low concentrations. The constant selectivity profile, despite declining conversion, indicates that the active sites responsible for dehydrative epoxidation remain functional, while sites involved in glycerol activation (e.g., Brønsted bases or oxygen vacancies) may gradually lose effectiveness. The absence of sharp drops in glycidol selectivity further indicates that no significant phase transformations, catalyst sintering, or partial volatilization occurred during the 27 h of reaction under the applied conditions. Instead, partial deactivation appears to be reversible or limited to surface fouling, which could potentially be mitigated by periodic oxidative regeneration. Moreover, the retention of product distribution over time highlights the selective nature and robustness of 15Cs/ZSM-5, making it suitable for extended continuous operation under ambient-pressure conditions. These findings emphasize that while catalyst lifetime could benefit from further stabilization strategies (e.g., anti-coking additives or Cs anchoring), the 15Cs/ZSM-5 formulation is fundamentally capable of maintaining high glycidol selectivity over long durations, even as activity gradually decreases.

3.2.3. *The effect of GHSV*

The influence of GHSV on the catalytic performance of 15Cs/ZSM-5 was investigated to understand how contact time affects the conversion–selectivity balance and productivity under continuous-flow conditions (Fig. 10). As GHSV increases, the residence time of reactants in the reactor decreases, potentially altering both reaction kinetics and product distribution. As shown in Fig. 10**a**, the carbon yield of glycidol increased significantly from ~12 % to ~44 % as GHSV rose from 500 to 1000 h^{-1}, indicating that shorter contact times favor glycidol formation by minimizing overreaction and secondary degradation. A maximum STY of ~0.71 mmol·g_{cat}^{-1}·h^{-1} was observed at 1500 h^{-1}, highlighting the benefit of higher throughput at intermediate space velocities. However, further increasing GHSV to 1900 h^{-1} led to a noticeable decline in both glycidol yield and STY, likely due to insufficient reaction time for complete glycerol conversion.

Fig. 10**b** further illustrates this trade-off. Glycerol conversion was highest at lower GHSV values (~85 %) and dropped to ~71 % at the highest GHSV tested, consistent with kinetic limitations at shorter residence times. At the same time, glycidol selectivity displayed a volcano-type trend, peaking at GHSV = 1000 h^{-1} (~52 %) and then declining with further increases. These observations suggest that excessive contact time (low GHSV) leads to overprocessing of glycidol or its intermediates,

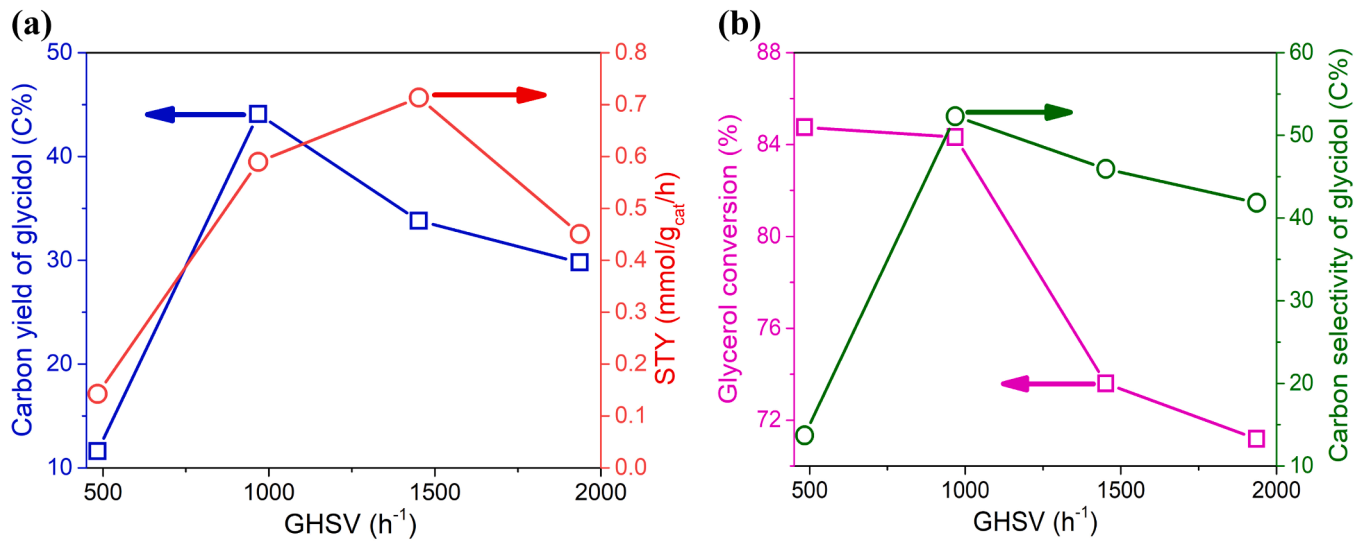

Fig. 10. The effect of GHSV on the glycidol yield, STY — (a) and glycerol conversion, glycidol selectivity — (b). Reaction conditions: 15Cs/ZSM-5 catalyst, 0.5 g, $T_{reactor}$ = 350 °C; P = 1 bar; C(GL) = 10 wt%, TOS = 8 h.

while too short residence times (high GHSV) limit the extent of glycerol activation. Together, these results indicate that an optimal GHSV around 1000–1500 h^{-1} maximizes both selectivity and productivity, balancing sufficient glycerol conversion with fast removal of glycidol to avoid secondary reactions. This further confirms the importance of tuning residence time and flow dynamics when designing continuous processes for selective oxygenate production.

3.2.4. *The effect of glycerol concentration*

The influence of glycerol feed concentration on glycidol selectivity, carbon yield, and productivity (STY) is shown in Fig. 11**a**. Increasing the concentration of glycerol from 5 to 20 wt% significantly enhanced both carbon selectivity (from ~42–67 %) and carbon yield (from ~40–65 %), indicating more efficient conversion to glycidol under moderately enriched feed conditions. This improvement can be attributed to enhanced interaction of glycerol with surface basic sites, improved adsorption kinetics, and higher surface coverage that facilitates the tandem dehydration-epoxidation mechanism. The trend, however, is not monotonic. Further increasing the glycerol concentration to 40 wt% resulted in a sharp drop in both selectivity (~53 %) and yield (~46 %), despite a continuous increase in STY, which peaked at 2.5 mmol·g_{cat}^{-1} ·h^{-1} . At elevated glycerol feed concentrations, the STY increases, indicating higher product formation per unit catalyst. Concomitantly, selectivity declines - consistent with the onset of secondary pathways and the coke formation detected by TGA (Fig. 13). While a full mechanistic dissection is beyond the scope of this study, the trends are compatible with local mass-transfer and/or vapor-liquid maldistribution effects at the catalyst surface under concentrated feeds, which can promote overconversion of glycidol. These observations align with reports on gas-phase glycerol conversion, where increasing feed strength typically results in higher productivity (STY) at the expense of selectivity [20–22]. Overall, 20 wt% glycerol represents an optimal feed concentration to maximize glycidol selectivity and yield, whereas higher concentrations improve short-term STY but exacerbate selectivity losses. Therefore, a careful balance must be achieved between feed concentration and catalytic surface dynamics to maintain high efficiency and suppress undesired transformations in continuous-flow systems.

3.2.5. *The effect of reaction pressure*

The influence of reaction pressure on catalytic performance was examined over a short TOS window (2–5 h) using the 15Cs/ZSM-5 catalyst, as shown in Fig. 11**b-c**. As the pressure increased from 2.0 to 2.75 bar, glycerol conversion improved markedly from ~31 % to ~64 % (Fig. 11**b**), indicating that higher partial pressures of glycerol and reaction intermediates enhance surface coverage and facilitate reaction kinetics under flow conditions. However, the glycerol conversion follows a volcano-type trend with increasing pressure (up to 4.5 bar), reaching a maximum of approximately 64 % at 2.75 bar. After 4 h time-on-stream at 4.5 bar, the glycerol conversion decreases to 47.5 %, which can be attributed to enhanced coke formation under higher pressure and extended reaction time. However, this gain in activity came at the cost of glycidol selectivity, which declined steadily from ~31 % to just ~4 % as pressure increased. This inverse relationship suggests that while elevated pressure accelerates glycerol conversion, it also promotes parallel and consecutive side reactions such as over-dehydration, aldol-type condensation, or glycidol degradation, leading to lower selectivity toward the desired epoxide [23–25].

This trade-off is further reflected in STY trends (Fig. 11**c**). The STY of glycidol peaked at ~1.7 mmol·g_{cat}^{-1} ·h^{-1} at 2.0 bar, but decreased sharply to ~0.1 mmol·g_{cat}^{-1} ·h^{-1} at 4.5 bar, demonstrating that product overconversion or instability dominates under higher-pressure regimes. Overall, these results highlight that low to moderate pressure (~1–2 bar) is optimal for glycidol production in continuous-flow systems using Cs-modified zeolites. Elevated pressures benefit glycerol activation but drastically reduce epoxide selectivity and STY, underscoring the need for fine control of operating conditions to suppress undesired reactivity.

3.3. *Reaction mechanism*

The catalytic behavior of Cs/ZSM-5 is strongly influenced by the acid-base bifunctionality of the material and by the intrinsic structural characteristics of the ZSM-5 support. The residual Brønsted acid sites of the ZSM-5 framework play a key role in the initial dehydration of glycerol to intermediate oxygenates, such as hydroxyacetone and allyl alcohol. These intermediates are subsequently epoxidized on Cs-induced basic sites, leading to the selective formation of glycidol. This tandem sequence is enabled by the unique structural and chemical properties of ZSM-5. The high SiO_2/Al_2O_3 ratio (1500) provides low intrinsic acidity and excellent hydrothermal stability, minimizing side reactions and ensuring catalyst durability at elevated temperatures. In addition, the well-defined MFI channel system (5.5 × 5.3 Å) allows precise control of intermediate residence time, promoting glycidol selectivity and

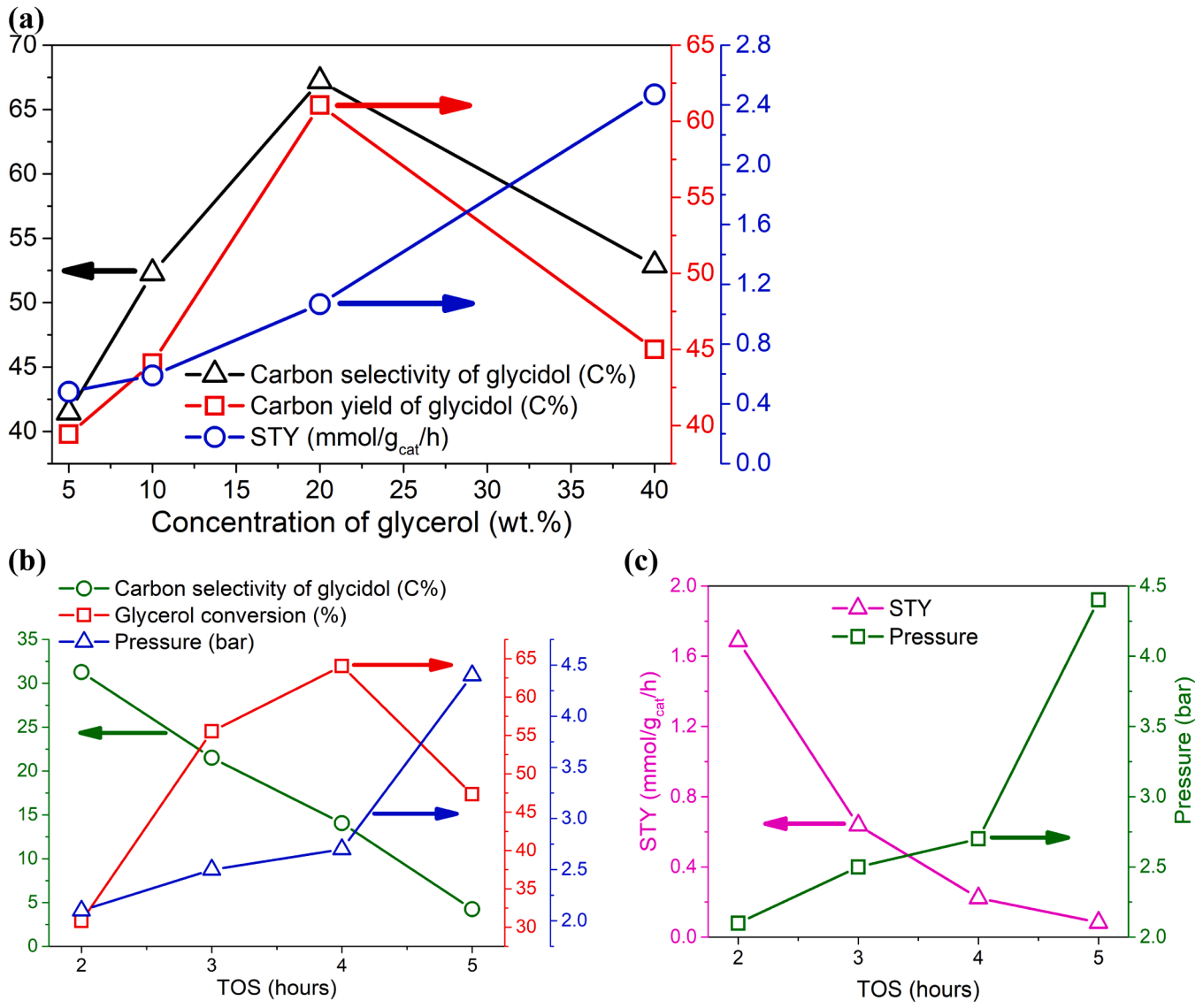

Fig. 11. (a) Effect of glycerol concentration on glycidol selectivity, yield, and STY. Reaction conditions: 15Cs/ZSM-5 catalyst, 0.5 g; T = 350 °C; P = 1 bar; FR(N_2) = 20 mL/min; FR(GL) = 2.34 mL/h; $GHSV_{total}$ = 968 h^{-1} ; TOS = 8 h. (b) Effect of reaction pressure on glycerol conversion and glycidol selectivity; (c) Effect of reaction pressure on glycidol STY. Reaction conditions for (b) and (c): 15Cs/ZSM-5 catalyst, 0.5 g; C(GL) = 20 wt%; FR(N_2) = 20 mL/min; T = 450 °C, FR(GL) = 2.34 mL/h; $GHSV_{total}$ = 968 h^{-1}.

suppressing undesired deep dehydration and polymerization pathways. Another critical factor is the relatively large crystal size of ZSM-5 compared to other zeolite types (e.g., Beta, Y, Mordenite), which reduces the contribution of external acid sites, thereby further limiting secondary reactions and enhancing stability under continuous operation. This combination of well-balanced acidity, optimized porosity, and structural robustness makes ZSM-5 an ideal support for Cs dispersion and enables highly selective one-step conversion of glycerol to glycidol.

The proposed reaction network (Fig. 12) reflects a complex interplay of parallel and consecutive reactions that occur during the gas-phase transformation of glycerol over *x*Cs/ZSM-5 catalysts. The primary route is a tandem dehydrative epoxidation, where glycerol undergoes stepwise dehydration on residual acidic sites of the zeolite support, followed by cyclization to glycidol on basic Cs-containing domains. This mechanistic scenario is supported by the dominance of glycidol in the product stream under optimized conditions and aligns with previous literature findings [7,23,26–28]. The detection of hydroxyacetone and its temporal increase during catalyst deactivation suggests its formation as a key intermediate or secondary product. This may result from incomplete epoxidation of glycerol or even from thermal decomposition of glycidol, as previously reported [29]. In fact, an inverse relationship between glycidol and hydroxyacetone concentrations was observed during TOS studies, indicating that hydroxyacetone may be both a precursor and a degradation product of glycidol under certain conditions. 1,2-propanediol likely arises from hydroxyacetone via transfer hydrogenation, further confirming that the acidic sites of the support are still catalytically active and influence selectivity by promoting parallel pathways. Similarly, allyl alcohol formation increases with temperature, and may participate in a secondary epoxidation pathway leading to glycidol. Based on our results, this epoxidation likely proceeds via the action of lattice oxygen species associated with Cs_2O and/or residual $CsNO_3$, even under an inert N_2 atmosphere, analogous to findings by Yasuda et al. [30] where lattice oxygen in NiO enabled CH_4 oxidation in reductive media.

The formation of phenol, particularly during the initial 2–3 h of reaction, supports the occurrence of Diels–Alder-type condensation between acrolein and acetone, both detected as minor intermediates. This pathway has also been documented over SAPO-11 and Al_2O_3–PO_4

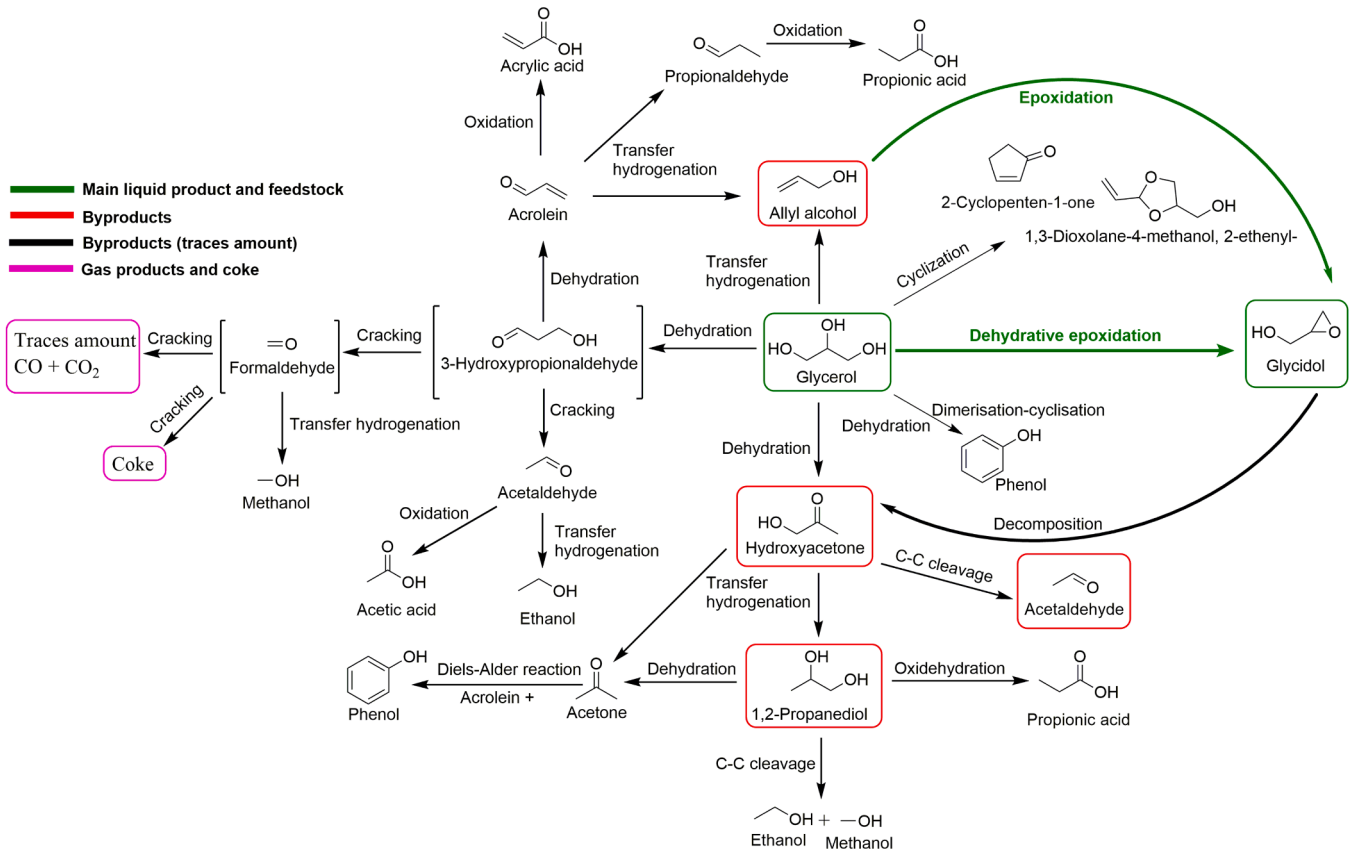

Fig. 12. Proposed reaction pathways from glycerol to glycidol over *x*Cs/ZSM-5 catalyst.

catalysts [31,32] with similar phenol selectivity (~8–10 %) at low TOS. The early appearance of phenol in our system corresponds with the period of highest catalyst activity, suggesting its formation is kinetically favored under fresh catalyst conditions but suppressed as surface deactivation occurs. Overall, the proposed mechanism confirms that dehydrative epoxidation is the dominant route to glycidol, but its efficiency is challenged by acid-catalyzed side reactions (leading to hydroxyacetone and acetaldehyde); C–C cleavage and condensation (resulting in formaldehyde, CO/CO_2, and phenol); and redox side-pathways (involving Cs-lattice oxygen in epoxidation of allyl alcohol). These mechanistic insights emphasize the need for precise tuning of acid–base balance and redox functionality in Cs/ZSM-5 systems to suppress byproduct formation while maintaining high glycidol selectivity.

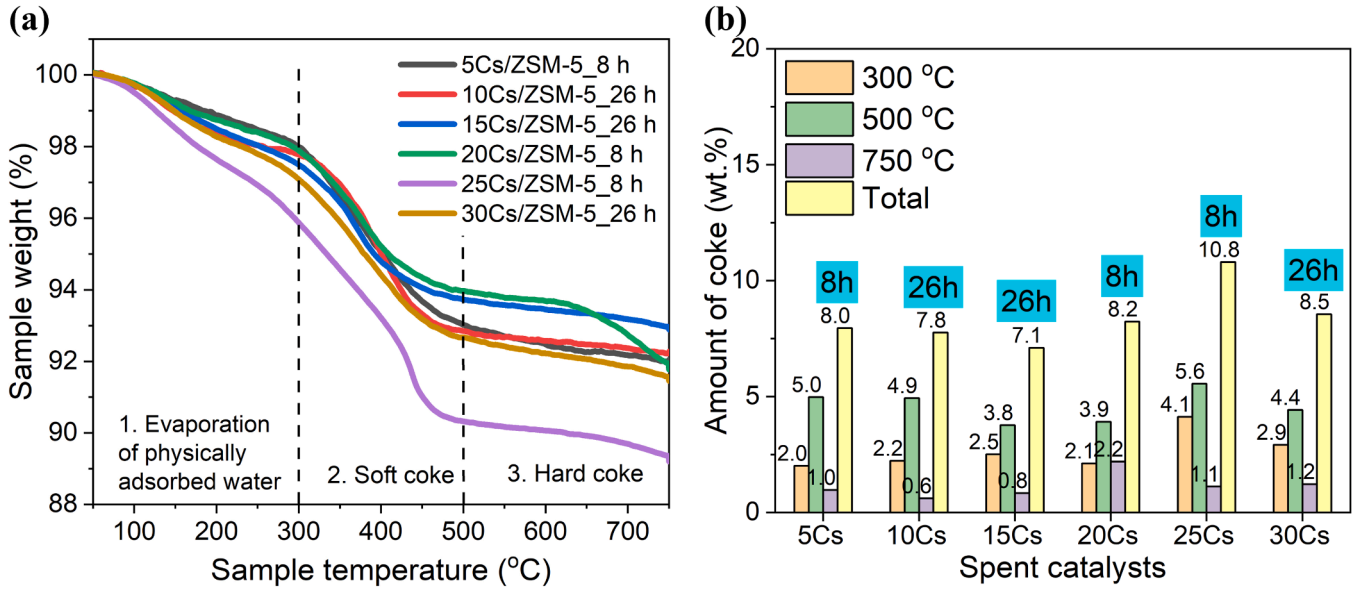

Fig. 13. TGA profiles for spent catalyst samples within 8 –26 h – (a) and the detected amount of coke – (b).

3.4. Catalyst deactivation and regeneration

It is known that catalysts can be deactivated due to of coking, sintering or poisoning [33,34]. Most of the catalysts under investigation exhibited progressive deactivation over TOS, primarily due to coke formation and deposition on their surfaces [35,36]. Thermogravimetric analysis (TGA) of spent catalysts (Fig. 13**a**) reveals the nature and extent of coke accumulation after 8 or 26 h of continuous operation. All samples exhibit three distinct weight-loss regions: (1) 100—300 °C, corresponding to physically adsorbed water, (2) 300–500 °C, attributed to soft coke (loosely bound, oxygen-rich species), and (3) > 500 °C, associated with hard coke (aromatic or graphitic-like species) [37,38]. The coke quantification (Fig. 13**b**) reveals that the total coke content ranged from 7.1 to 10.8 wt% depending on Cs loading and TOS. Notably, the 15Cs/ZSM-5 catalyst exhibited one of the lowest total coke amounts (7.1 wt%) after 26 h TOS, with only 0.8 wt% attributable to hard coke (oxidized at 750 °C). In contrast, 25Cs/ZSM-5 accumulated the highest coke amount (10.8 wt%) within just 8 h, largely dominated by soft coke. This confirms that excessive Cs loading can accelerate condensation and surface fouling, likely due to increased viscosity, restricted pore access, or unselective side reactions on overly basic surfaces. Interestingly, despite the presence of some hard coke, the 15Cs/ZSM-5 catalyst maintained stable glycidol selectivity and was successfully regenerated (see Fig. 14), indicating that its deactivation is primarily physical (pore blockage) rather than chemical (active site loss). Furthermore, catalysts with lower or excessive Cs content not only accumulated more coke but also demonstrated reduced selectivity and stability, highlighting the importance of tuning the Cs loading for optimal coke resistance. These results confirm that 15Cs provides an optimal balance, ensuring high activity, minimal coke formation, and long-term performance. While coke formation is inevitable in glycerol-based systems, the type and extent of deposition are strongly influenced by catalyst composition. The relatively low hard coke content on 15Cs/ZSM-5 suggests that oxidative regeneration is feasible, further enhancing its potential for industrial continuous-flow applications.

The performance of the regenerated 15Cs/ZSM-5 catalyst was evaluated and compared to the fresh material under identical reaction conditions (Fig. 14) to assess its reusability and regeneration efficiency. After oxidative treatment of the spent catalyst, a notable recovery in activity and selectivity was observed. As shown in Fig. 14**a**, the regenerated catalyst achieved ~52 % glycerol conversion within TOS = 8 h, a substantial improvement over the fresh sample, whose conversion decreased steadily to ~28 % due to deactivation. Simultaneously, the carbon selectivity to glycidol was also enhanced and stabilized in the range of 40–45 %, compared to the fresh catalyst, which was ~38–40 %. This improvement can be primarily attributed to thermal effects during the regeneration procedure. The thermal treatment applied during regeneration may have induced further decomposition of residual $CsNO_3$ into Cs_2O. The formation of additional Cs_2O on the catalyst surface likely enhanced the density and strength of basic sites, which are known to promote the epoxidation step from glycerol to glycidol. This gradual transformation of $CsNO_3$ into Cs_2O, particularly under prolonged calcination at elevated temperatures, might have led to the formation of a more catalytically active and stable surface phase distribution, ultimately improving both the selectivity and long-term performance of the catalyst. This assumption is supported by our previous study [7], where detailed characterization of regenerated and spent catalysts revealed a significant decrease in $CsNO_3$ content in regenerated samples, as confirmed by XRD analysis. Moreover, it is plausible that some of the acid sites, which typically facilitate undesired side reactions such as over-dehydration to hydroxyacetone or C–C bond cleavage to light oxygenates, were partially deactivated or passivated during the initial TOS. As a result, after regeneration, the catalyst surface exhibited a more favorable acid-base balance, suppressing non-selective pathways and promoting the selective dehydrative epoxidation of glycerol. This explanation aligns with the observed reduction in hydroxyacetone and acetaldehyde formation, further confirming the enhanced selectivity of the regenerated catalyst toward glycidol.

Further evidence of regeneration success is presented in Fig. 14**b**, where both carbon yield and STY of glycidol were significantly higher for the regenerated catalyst. The STY peaked at ~1.6 $mmol \cdot g_{cat}^{-1} \cdot h^{-1}$, which is substantially higher than the maximum value observed for the fresh sample (~1.1 $mmol \cdot g_{cat}^{-1} \cdot h^{-1}$). This improvement can be attributed to restored diffusion pathways, reopened pore structures, and re-exposure of active epoxidation sites after oxidative coke removal. These results demonstrate that 15Cs/ZSM-5 exhibits excellent regenerability, with restored or even enhanced catalytic performance after coke combustion. The ability to maintain selectivity and productivity after regeneration confirms the structural resilience of the catalyst and supports its suitability for long-term use in industrial continuous-flow applications, especially when paired with periodic regeneration strategies to manage coke buildup.

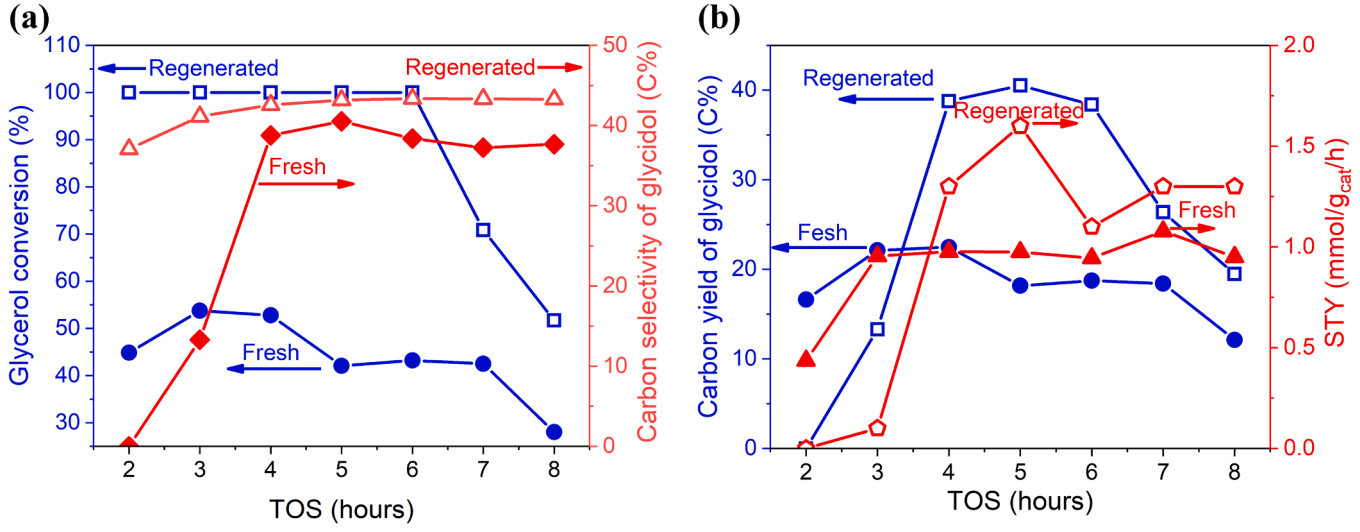

Fig. 14. Comparison of fresh and regenerated 15Cs/ZSM-5 catalysts: dependence of glycerol conversion and glycidol selectivity — (a); dependence of yield of glycidol and STY on TOS — (b). Reaction conditions: TOS = 8 h; catalyst amount = 0.5 g; $T_{reactor}$ = 400 °C; P = 1 bar; FR(N_2) = 20 mL/min; FR(GL) = 2.34 mL/h; $GHSV_{total}$ = 968 h^{-1}.

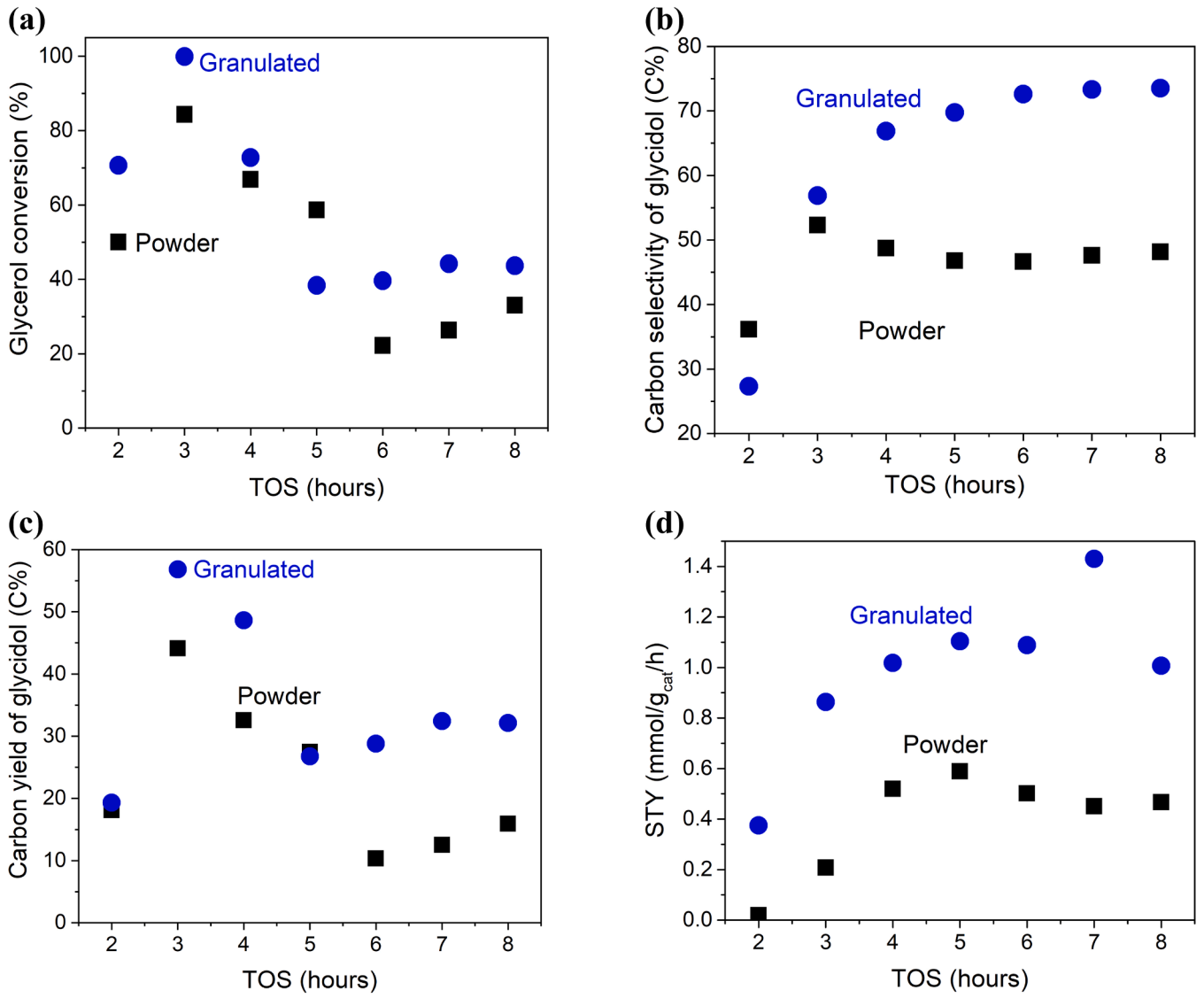

Fig. 15. Comparison of powder and granulated (250–400 μm) 15Cs/ZSM-5 catalysts: (a, b) glycerol conversion and glycidol selectivity as a function of TOS; (c, d) glycidol yield and STY as a function of TOS. Reaction conditions: $T_{reactor}$ = 350 °C; TOS = 8 h; catalyst amount = 0.5 g; P = 1 bar; FR(N_2) = 20 mL/min; FR(GL) = 2.34 mL/h; $GHSV_{total}$ = 968 h^{-1}.

3.5. *The effect of catalyst granulation*

The effect of catalyst form on the one-step conversion of glycerol to glycidol was assessed by comparing powdered and granulated 15Cs/ZSM-5 catalysts under identical reaction conditions (Fig. 15). The granulated catalyst exhibited significantly superior performance across all key metrics: glycerol conversion, glycidol selectivity, carbon yield, and STY at TOS = 8 h. As shown in Fig. 15**a**, the granulated catalyst maintained ~100 % glycerol conversion in the early stages and stabilized around 45 %, while the powdered version declined from ~85 % to just ~33 % by the end of the run. The improved stability in the granulated form likely results from better mechanical integrity, reduced pressure drop, and enhanced heat and mass transfer within the packed-bed reactor.

In terms of glycidol selectivity (Fig. 15**b**), the granulated catalyst steadily increased and stabilized at 74 %, significantly outperforming the powder form, which plateaued below 50 %. This indicates that the larger particle size and structured porosity in the granules support more favorable reaction environments, minimizing overreaction and coke precursors. Likewise, glycidol carbon yield and STY (Fig. 15**c-d**) were consistently higher for the granulated sample, peaking at ~1.4 mmol·g_{cat}^{-1}·h^{-1} in STY compared to just 0.6 for the powder. The enhanced yield and productivity further highlight the practical importance of catalyst shaping and pelletization for industrial applications, particularly for long-term continuous-flow processes where thermal stability, pressure drop, and resistance to channeling are critical.

3.6. *Catalyst stability*

The long-term catalytic behavior of 15Cs/ZSM-5 was evaluated over 70 h of continuous operation at 550 °C, aiming to test its thermal stability and product selectivity under intensified conditions. As shown in Fig. 16**a**, the catalyst initially maintained complete glycerol conversion (~100 %) for over 39 h, followed by a gradual decline to ~80 % by 70 h TOS. Despite the slight decrease in conversion, the catalyst exhibited remarkable stability considering the elevated temperature and prolonged exposure. The glycidol yield peaked around 20–30 h TOS at ~51 %, before slowly declining to ~34 % by the end of the run. This modest drop can be attributed to gradual pore blockage from coke or partial sintering, yet it still reflects strong resistance to thermal degradation and secondary reactions. The consistently high glycidol yield demonstrates that the active dehydrative epoxidation sites remain

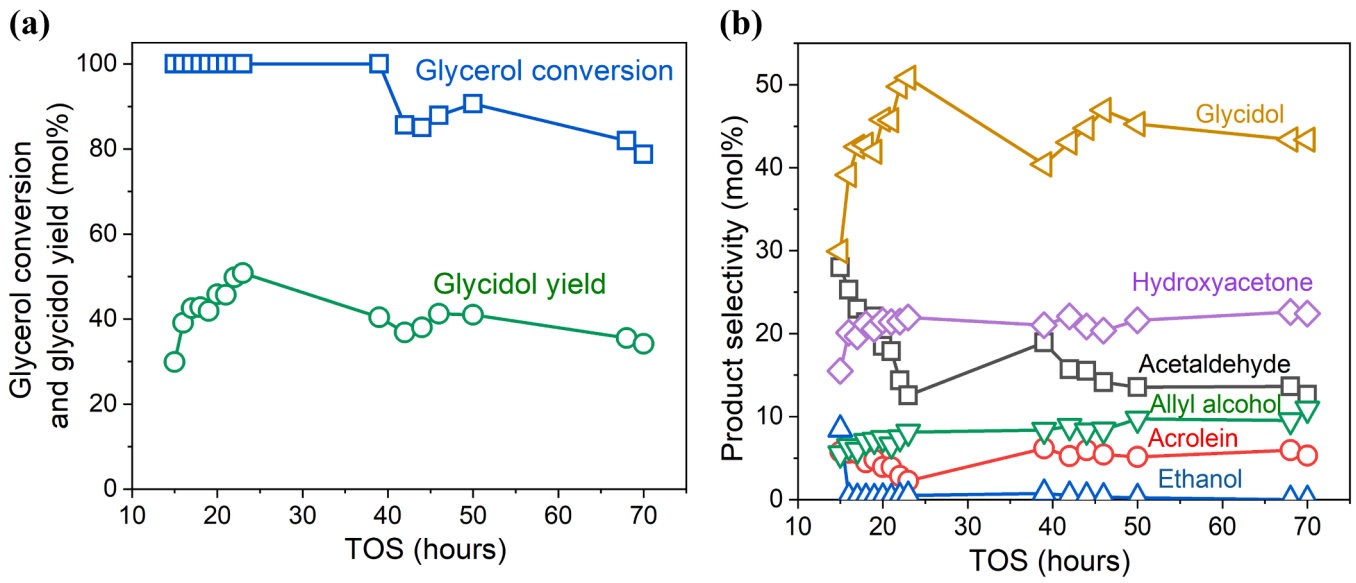

Fig. 16. The effect of TOS on the glycerol conversion and glycidol yield – (a) and product selectivity – (b). Reaction conditions: 15Cs/ZSM-5 catalyst, 0.5 g, $T_{reactor}$ = 550 °C; C(GL) = 10 wt%; FR(N_2) = 20 mL/min; FR(GL) = 2.34 mL/h; $GHSV_{total}$ = 968 h^{-1}; TOS = 70 h.

functional for extended durations, even under demanding thermal conditions.

The corresponding product distribution trends (Fig. 16**b**) further support the robustness of 15Cs/ZSM-5. Glycidol remained the dominant product throughout the 70 h period, maintaining selectivity values between 51 % and 43 %. The main byproducts included hydroxyacetone, acetaldehyde, and allyl alcohol, which together accounted for most of the carbon not converted to glycidol. Notably, hydroxyacetone selectivity increased slightly as glycidol selectivity declined, consistent with the previously discussed reversible relationship between these species, possibly via glycidol thermal degradation. Low and stable levels of acrolein and ethanol further confirm that deep dehydration and C–C cracking pathways were successfully suppressed by the tuned acid-base surface environment of the 15Cs/ZSM-5 catalyst. Importantly, no abrupt shifts in product profile were observed over the 70 h run, indicating steady-state behavior and minimal structural degradation. These findings confirm that 15Cs/ZSM-5 is thermally and catalytically stable over extended operation at high temperatures, reinforcing its viability for industrial-scale glycidol production in continuous mode, especially where periodic regeneration is possible.

The initial increase in catalytic activity during the first several hours (Fig. 16) is attributed to the activation of $CsNO_3$ species on the ZSM-5 surface. At the beginning of the reaction, partial decomposition and redistribution of $CsNO_3$ lead to the formation of well-dispersed basic sites, which enhance the catalytic performance for glycerol dehydration to glycidol. This activation process is accompanied by the removal of residual moisture and surface impurities, improving active site accessibility and mass transport. The subsequent decline in activity after reaching the maximum conversion is primarily due to catalyst deactivation caused by (i) the gradual decomposition and restructuring of the $CsNO_3$ active phase at elevated temperatures, which decreases the number of active basic sites, and (ii) coke deposition resulting from secondary condensation and polymerization of glycerol-derived intermediates, leading to partial pore blockage and restricted access to active centers. This behavior aligns with the two-stage deactivation pattern discussed earlier (**Section 3.2**), where an initial increase in activity is followed by a slower but continuous decline.

Partial Cs loss may occur through volatilization at elevated temperatures (550 °C) or migration within the zeolite framework. XRD analysis of the spent catalysts (Fig. S2) indicates changes in the $CsNO_3$ phase intensity, suggesting Cs redistribution and possible volatilization. This effect will be systematically investigated in future studies, including the use of different alkali metals (Li, Na, K, Rb) and their oxides or salts, to enhance catalyst stability.

4. Conclusions

This study confirms the viability of using $CsNO_3$-modified ZSM-5 zeolite catalysts for the efficient one-step gas-phase conversion of glycerol to glycidol under ambient pressure. A broad range of process and material parameters was systematically evaluated, including Cs loading, reaction temperature, glycerol concentration, GHSV, pressure, catalyst form (powder vs. granules), as well as catalyst deactivation and regeneration behavior. Among the investigated formulations, the granulated 15Cs/ZSM-5 catalyst exhibited superior performance, achieving a maximum glycidol selectivity of 74.0 C% at 350 °C after 8 h TOS with 10 wt% glycerol, and a peak STY of 2.5 $mmol \cdot g_{cat}^{-1} \cdot h^{-1}$ at 40 wt% glycerol concentration. While glycerol conversion gradually declined during extended operation, glycidol selectivity remained stable over 70 h, demonstrating the durability of the active sites. Catalyst characterization and performance analysis revealed that the enhanced activity and selectivity of 15Cs/ZSM-5 stem from a synergistic combination of structural and chemical features: moderate textural degradation, sufficient mesoporosity enabling effective mass transfer, high Cs dispersion generating accessible basic sites, and a partially disordered zeolite framework that supports selective tandem dehydration-epoxidation. Furthermore, regeneration experiments confirmed that the catalyst activity and selectivity could be restored or even slightly improved through oxidative treatment, attributed to additional $CsNO_3$ decomposition into catalytically active Cs_2O. In summary, 15 wt% Cs represents the optimal loading for balancing surface basicity, pore accessibility, and catalytic stability, making this material a promising candidate for scalable, continuous glycidol production from renewable glycerol feedstock.

CRediT authorship contribution statement

Andrii Kostyniuk: Writing – review & editing, Writing – original draft, Visualization, Validation, Supervision, Software, Resources, Project administration, Methodology, Investigation, Funding acquisition, Formal analysis, Data curation, Conceptualization. **Blaž Likozar:** Writing – review & editing, Supervision, Project administration,

Funding acquisition. **Anže Prašnikar:** Writing – review & editing, Investigation, Data curation.

Declaration of Competing Interest

The authors declare that they have no known competing financial interests or personal relationships that could have appeared to influence the work reported in this paper.

Acknowledgements

The authors acknowledge financial support from D.O.T.W. and the Slovenian Research Agency (ARIS) through the GRAVITACIJA (POLY-LOOP) program, as well as research core funding No. P2–0152, J2–2492, J2–1723, and J7–1816. The authors are also thankful to Urška Kavčič for N_2 physisorption measurements, Mr. Edi Kranjc (XRD analysis), and Dr. Goran Dražić (TEM analysis).

Appendix A. Supporting information

Supplementary data associated with this article can be found in the online version at doi:10.1016/j.jece.2025.120416.

Data Availability

Data will be made available on request.

References

[1] G.D. Fao, H.N. Catherine, C.-H. Huang, Y.-L. Lee, J.-C. Jiang, C. Hu, Unraveling the effects of P and S doping over g-C3N4 in strengthening Lewis basicity for CO2/glycerol conversion: a theoretical and experimental study, Carbon 201 (2023) 129–140, https://doi.org/10.2139/ssrn.4142245.
[2] S. He, T.S. Kramer, D.S. Santosa, A. Heeres, H.J. Heeres, Catalytic conversion of glycerol and co-feeds (fatty acids, alcohols, and alkanes) to bio-based aromatics: remarkable and unprecedented synergetic effects on catalyst performance, Green. Chem. 24 (2022) 941–949, https://doi.org/10.1039/d1gc03531b.
[3] IEA, Global biofuel production in 2019 and forecast to 2025, Paris, 2020⟨https://www.iea.org/data-and-statistics/charts/global-biofuel-production-in-2019-and-forecast-to-2025⟩.
[4] P. Cardillo, M. Nebuloni, Theoretical and calorimetric evaluation of thermal stability of glycidol, J. Loss Prev. Process Ind. 4 (1991) 242–245, https://doi.org/10.1016/0950-4230(91)85007-G.
[5] ⟨https://www.acs.org/content/acs/en/molecule-of-the-week/archive/g/glycidol.html⟩, Molecule of the Week Archive Glycidol, ACS. (2019).
[6] C. Muzyka, J.C.M. Monbaliu, Perspectives for the Upgrading of Bio-Based Vicinal Diols within the Developing European Bioeconomy, ChemSusChem 15 (2022), https://doi.org/10.1002/cssc.202102391.
[7] A. Kostyniuk, D. Bajec, P. Djinović, B. Likozar, One-step synthesis of glycidol from glycerol in a gas-phase packed-bed continuous flow reactor over HZSM-5 zeolite catalysts modified by CsNO3, Chem. Eng. J. 394 (2020) 124945, https://doi.org/10.1016/j.cej.2020.124945.
[8] R. Sharma, V. Chandola, S. Bhat, Glob. Glycidol Mark. Res. Rep. 2033 (2025). ⟨https://growthmarketreports.com/report/glycidol-market-global-industry-analysis⟩.
[9] P. Prete, D. Cespi, F. Passarini, C. Capacchione, A. Proto, R. Cucciniello, Glycidol syntheses and valorizations: boosting the glycerol biorefinery, Curr. Opin. Green. Sustain. Chem. 35 (2022) 100624, https://doi.org/10.1016/j.cogsc.2022.100624.
[10] R.J. Davis, New perspectives on basic zeolites as catalysts and catalyst supports, J. Catal. 216 (2003) 396–405, https://doi.org/10.1016/S0021-9517(02)00034-9.
[11] C.B. Dartt, M.E. Davis, Applications of zeolites to fine chemicals synthesis, Catal. Today 19 (1994) 151–186, https://doi.org/10.1016/0920-5861(94)85006-2.
[12] T.Y. Kim, J. Baek, C.K. Song, Y.S. Yun, D.S. Park, W. Kim, J.W. Han, J. Yi, Gas-phase dehydration of vicinal diols to epoxides: Dehydrative epoxidation over a Cs/SiO2 catalyst, J. Catal. 323 (2015) 85–99, https://doi.org/10.1016/j.jcat.2014.12.023.
[13] W. Kim, W. Shin, K.J. Lee, Y.S. Cho, H.S. Kim, I.N. Filimonov, 2,3-Butanediol dehydration catalyzed by silica-supported alkali phosphates, Appl. Catal. A Gen. 570 (2019) 148–163, https://doi.org/10.1016/j.apcata.2018.08.015.
[14] A. Kostyniuk, D. Bajec, P. Djinović, B. Likozar, Allyl alcohol production by gas phase conversion reactions of glycerol over bifunctional hierarchical zeolite-supported bi- and tri-metallic catalysts, Chem. Eng. J. 397 (2020) 125430, https://doi.org/10.1016/j.cej.2020.125430.
[15] L.B. Sun, X.Q. Liu, H.C. Zhou, Design and fabrication of mesoporous heterogeneous basic catalysts, Chem. Soc. Rev. 44 (2015) 5092–5147, https://doi.org/10.1039/c5cs00090d.
[16] P. Käßner, M. Baerns, Comparative characterization of basicity and acidity of metal oxide catalysts for the oxidative coupling of methane by different methods, Appl. Catal. A Gen. 139 (1996) 107–129, https://doi.org/10.1016/0926-860X(95)00335-5.
[17] K. Tanabe, T. Yamaguchi, Basicity and acidity of solid surfaces, J. Res. Inst. Catal. Hokkaido Univ. 11 (1963) 179–184.
[18] D. Barthomeuf, Basic zeolites: characterization and uses in adsorption and catalysis, Catal. Rev. Sci. Eng. 38 (1996) 521–612, https://doi.org/10.1080/01614949608006465.
[19] A. Kostyniuk, D. Bajec, B. Likozar, One-step synthesis of ethanol from glycerol in a gas phase packed bed reactor over hierarchical alkali-treated zeolite catalyst materials, Green. Chem. 22 (2020) 753–765, https://doi.org/10.1039/c9gc03262b.
[20] M.H. Haider, N.F. Dummer, D.W. Knight, R.L. Jenkins, M. Howard, J. Moulijn, S. H. Taylor, G.J. Hutchings, Efficient green methanol synthesis from glycerol, Nat. Chem. 7 (2015) 1028–1032, https://doi.org/10.1038/nchem.2345.
[21] S. Thanasilp, J.W. Schwank, V. Meeyoo, S. Pengpanich, M. Hunsom, One-pot oxydehydration of glycerol to value-added compounds over metal-doped SiW/HZSM-5 catalysts: Effect of metal type and loading, Chem. Eng. J. 275 (2015) 113–124, https://doi.org/10.1016/j.cej.2015.04.010.
[22] J. Remón, J.R. Giménez, A. Valiente, L. García, J. Arauzo, Production of gaseous and liquid chemicals by aqueous phase reforming of crude glycerol: Influence of operating conditions on the process, Energy Convers. Manag 110 (2016) 90–112, https://doi.org/10.1016/j.enconman.2015.11.070.
[23] M.R. Nimlos, S.J. Blanksby, X. Qian, M.E. Himmel, D.K. Johnson, Mechanisms of glycerol dehydration, J. Phys. Chem. A. 110 (2006) 6145–6156, https://doi.org/10.1021/jp060597q.
[24] B. Katryniok, S. Paul, V. Belliere-Baca, P. Rey, F. Dumeignil, Glycerol dehydration to acrolein in the context of new uses of glycerol, Green. Chem. 12 (2010) 2079–2098, https://doi.org/10.1039/c0gc00307g.
[25] G.-Y. Yang, Y.-H. Ke, H.-F. Ren, C.-L. Liu, R.-Z. Yang, W.-S. Dong, The conversion of glycerol to lactic acid catalyzed by ZrO2-supported CuO catalysts, Chem. Eng. J. 283 (2016) 759–767, https://doi.org/10.1016/j.cej.2015.08.027.
[26] W. Sun, J. Liu, X. Chu, C. Zhang, C. Liu, Theoretical study of the dynamics and thermal mechanisms of the reaction: dehydration of glycerol to glycidol, J. Mol. Struct. Theochem. 942 (2010) 38–42, https://doi.org/10.1016/j.theochem.2009.11.030.
[27] T. Laino, C. Tuma, A. Curioni, E. Jochnowitz, S. Stolz, A revisited picture of the mechanism of glycerol dehydration, J. Phys. Chem. A. 115 (2011) 3592–3595, https://doi.org/10.1021/jp201078e.
[28] R.C.R. Santos, D.M.V. Braga, A.N. Pinheiro, E.R. Leite, V.N. Freire, E. Longhinotti, A. Valentini, Role of Cu, Ni and Co metals in the acidic and redox properties of Mo catalysts supported on Al2O3 spheres for glycerol conversion, Catal. Sci. Technol. 6 (2016) 4986–5002, https://doi.org/10.1039/C6CY00096G.
[29] F. Ullmann, Ullmann's Fine Chemicals, 2014.
[30] S. Yasuda, R. Osuga, Y. Kunitake, K. Kato, A. Fukuoka, H. Kobayashi, M. Gao, J. ya Hasegawa, R. Manabe, H. Shima, S. Tsutsuminai, T. Yokoi, Zeolite-supported ultra-small nickel as catalyst for selective oxidation of methane to syngas, Commun. Chem. 3 (2020) 1–8, https://doi.org/10.1038/s42004-020-00375-0.
[31] I. Martinuzzi, Y. Azizi, J.F. Devaux, S. Tretjak, O. Zahraa, J.P. Leclerc, Reaction mechanism for glycerol dehydration in the gas phase over a solid acid catalyst determined with on-line gas chromatography, Chem. Eng. Sci. 116 (2014) 118–127, https://doi.org/10.1016/j.ces.2014.04.030.
[32] W. Suprun, M. Lutecki, T. Haber, H. Papp, Acidic catalysts for the dehydration of glycerol: Activity and deactivation, J. Mol. Catal. A Chem. 309 (2009) 71–78, https://doi.org/10.1016/j.molcata.2009.04.017.
[33] M. Milina, S. Mitchell, P. Crivelli, D. Cooke, J. Pérez-Ramírez, Mesopore quality determines the lifetime of hierarchically structured zeolite catalysts, Nat. Commun. 5 (2014) 1–10, https://doi.org/10.1038/ncomms4922.
[34] J. Zhang, Y. Li, H. Song, L. Zhang, Y. Wu, Y. He, L. Ma, J. Hong, A. Tayal, N. Marinkovic, D.E. Jiang, Z. Li, Z. Wu, F. Polo-Garzon, Tuning metal-support interactions in nickel-zeolite catalysts leads to enhanced stability during dry reforming of methane, Nat. Commun. 15 (2024) 8566, https://doi.org/10.1038/s41467-024-50729-8.
[35] H.E. Van Der Bij, B.M. Weckhuysen, Phosphorus promotion and poisoning in zeolite-based materials: synthesis, characterisation and catalysis, Chem. Soc. Rev. 44 (2015) 7406–7428, https://doi.org/10.1039/c5cs00109a.
[36] G. Pauletto, A. Vaccari, G. Groppi, L. Bricaud, P. Benito, D.C. Boffito, J.A. Lercher, G.S. Patience, FeCrAl as a catalyst support, Chem. Rev. 120 (2020) 7516–7550, https://doi.org/10.1021/acs.chemrev.0c00149.
[37] M. Díaz, E. Epelde, J. Valecillos, S. Izaddoust, A.T. Aguayo, J. Bilbao, Coke deactivation and regeneration of HZSM-5 zeolite catalysts in the oligomerization of 1-butene, Appl. Catal. B Environ. 291 (2021) 120076, https://doi.org/10.1016/j.apcatb.2021.120076.
[38] N. Kosinov, E.A. Uslamin, F.J.A.G. Coumans, A.S.G. Wijpkema, R.Y. Rohling, E.J. M. Hensen, Structure and evolution of confined carbon species during methane dehydroaromatization over Mo/ZSM-5, ACS Catal. 8 (2018) 8459–8467, https://doi.org/10.1021/acscatal.8b02491.